Check for updates

SEDIMENTOLOGY the journal of the International Association of Sedimentologists IAS

Sedimentology (2024) **71**, 319–354 doi: 10.1111/sed.13138

Seismic stratigraphy of Late Pleistocene incised valleys and adjacent environments, eastern Central Luconia Province, offshore north-west Borneo

HABIBAH HANAN MAT YUSOFF*,†, HOWARD D. JOHNSON*, LIDIA LONERGAN*, ALEXANDER C. WHITTAKER* and AZLI ABU BAKAR‡
**Department of Earth Science and Engineering, Imperial College, London SW7 2BP, UK (E-mail: habibah.mat@umt.edu.my)*
†Faculty of Science and Marine Environment, Universiti Malaysia Terengganu, Kuala Nerus 21030, Malaysia
‡PETRONAS, KLCC, Kuala Lumpur, Malaysia

Associate Editor – Christopher Fielding

ABSTRACT

Incised valleys are commonly investigated based on outcrop, modern setting and seismic data, which are often limited by data availability, especially for broad (*ca* >100 km wide) shelf settings. Consequently, few have described complete depositional systems of the incised valleys, especially those linked to their corresponding modern rivers in a source-to-sink framework to determine comprehensive controlling factors. This study documents Late Quaternary incised valleys and their characteristics in the Balingian – Central Luconia shelf based on regionally-extensive three-dimensional seismic data, two-dimensional high-resolution seismic data and boreholes. The three-dimensional seismic data show that the main Tatau incised valley and tributary Suai incised valley fed the Tatau–Suai shelf-edge delta. The Tatau incised valley is interpreted as the main incised valley based on its broader width, thicker infill, two-tier stratigraphic architecture and its larger drainage basin area compared to the tributary Suai incised valley. The Tatau incised valley shifted its direction towards an active tectonic lineament (West Baram Line) and bypassed sediments to the deep-water via a series of upper slope channels. The Tatau incised valley system comprises the following elements: (i) an upstream segment characterized by rivers dissecting an uplifted hinterland comprising Neogene sedimentary rocks, humid-tropical vegetation, monsoonal climate, extremely high river discharge and sediment supply; (ii) a midstream segment comprising an emergent, vegetated (tropical rainforest to mangroves) and relatively narrow (*ca* 150 to 200 km wide) shelf, which was characterized by basinward-increasing, tectonically-driven accommodation space, valley incision and deposition; (iii) a downstream segment with increasing tidal-influence where the Tatau and its tributary valley merged; and (iv) a short (15 to 20 km), narrow (10 to 15 km), tectonically-controlled shelf-edge delta and channelized upper slope. This study demonstrates the value of documenting an incised valley system in the context of its broader source-to-sink setting, which may provide a useful analogue for ancient incised valleys in comparable geological settings.

Keywords Central Luconia Province, incised valleys, Late Quaternary, shelf-edge delta, Sunda Shelf, three-dimensional seismic.

© 2023 The Authors. *Sedimentology* published by John Wiley & Sons Ltd on behalf of International Association of Sedimentologists.
This is an open access article under the terms of the Creative Commons Attribution-NonCommercial License, which permits use, distribution and reproduction in any medium, provided the original work is properly cited and is not used for commercial purposes.

INTRODUCTION

Incised valleys have been widely studied in various climate settings and through different geological time-periods. Incised valleys are recognized based on dimensions, regionally extensive basal erosion surfaces, and distinctive facies types from those in adjacent and preceding strata (Van Wagoner *et al.*, 1990; Zaitlin *et al.*, 1994; Best & Ashworth, 1997; Hampson *et al.*, 1999; Reynaud *et al.*, 1999; Posamentier, 2001; Gibling, 2007; Catuneanu *et al.*, 2009). Incised valley formation is closely related to relative sea-level changes, most notably with valley incision occurring during sea-level fall and valley infill mainly coinciding with periods of sea-level rise (Zaitlin *et al.*, 1994). Thus, incised valleys are important for understanding past sea-level changes and reconstructing depositional histories, palaeogeographies and source-to-sink systems (Posamentier *et al.*, 1988; Dalrymple, 1994; Shanley & McCabe, 1994; Zaitlin *et al.*, 1994; Mattheus & Rodriguez, 2011; Blum *et al.*, 2013; Alqahtani *et al.*, 2015; Bhattacharya *et al.*, 2016).

Some of the best documented incised valleys are found in the Quaternary, when glaciation was a major control on eustatic sea-level changes, especially in low latitude settings where shelves were not glaciated. For example, in the Late Pleistocene of Southeast Asia, incised valleys were abundant on the wide (*ca* 600 km) and stable Sunda Shelf, when sea-level was −120 m below the present level, causing widespread subaerial erosion (Voris, 2000). Previous studies on these Late Pleistocene incised valleys have investigated the following aspects: (i) relatively short segments of the single major trunk mostly concentrated in the midstream reach; (ii) longer river systems (>1000 km); (iii) a single major trunk river draining relatively distant hinterlands; (iv) large (*ca* 100 000 km^2) palaeo-drainages (for example, palaeo-Chao Phraya-Johore and palaeo-North Sunda rivers; Posamentier, 2001; Miall, 2002; Darmadi *et al.*, 2007; Puchała *et al.*, 2011; Reijenstein *et al.*, 2011; Alqahtani *et al.*, 2015, 2017; Fig. 1). These examples are located in relatively tectonically-stable parts of the Sunda Shelf, often far distant (hundreds of kilometres) from their catchment areas.

However, previous incised valley studies have lacked the complete depositional system to observe how the downstream incised valley changes relate to the controlling factors (for example, sediment supply, tectonics). This study focuses on the Quaternary coastal plain depositional system in the Central Luconia and Balingian provinces, offshore north-west Borneo, which displays a different style of Pleistocene incised valley to those described previously (Fig. 1). Here, the incised valleys are located on a relatively narrow part of the Sunda shelf (*ca* 300 km wide) and are characterized as follows: (i) shorter river systems, located between the major palaeo-Rajang and Baram rivers (200 to 350 km); (ii) multiple river systems draining the nearby and recently uplifted hinterland (Rajang Range fold–thrust belt); and (iii) a shelf edge that is partly defined by a major and long-lived tectonic lineament, the West Baram Line (WBL; Fig. 1).

This study aims to document Late Pleistocene incised valleys and the adjacent depositional elements in the eastern Central Luconia Province (CLP) by: (i) evaluating incised valley stratigraphic architecture and depositional evolution from the upper to lower coastal plain to the shelf edge; (ii) quantifying the dimensions and geometries of incised valleys and shelf-edge delta; and (iii) determining the larger scale geological controls on the youngest Late Pleistocene incised valleys in the CLP. The evaluation uses a diverse subsurface dataset, which crucially includes a regionally-extensive three-dimensional seismic data (*ca* 90 000 km^2) enabling a source-to-sink analysis of a Late Pleistocene incised valley network (Figs 1 and 2). This is supported by seven site survey reports (some of which include two-dimensional high-resolution seismic data) and 17 boreholes described in the geotechnical reports (the boreholes extend up to 50 to 150 m below seabed), which cover most of the CLP shelf (Fig. 2). The detailed mapping shows a network of multiple, *ca* 0.3 to 12 km wide and generally northward-trending incised valleys, which receive sediments from various sizes of palaeo-drainages (Fig. 2).

REGIONAL GEOLOGICAL SETTING

North-west Borneo has a complex geological history. The interior consists of deep-water clastic sediments within an Eocene to Late Oligocene fold–thrust belt, which forms the Rajang–Crocker Range (Fig. 2). The north-west Borneo coastal plain is dominated by the Rajang river and delta (Staub & Gastaldo, 2003), plus numerous smaller rivers (for example, Baram, Tatau, Kemena and Mukah rivers); all of these rivers have drainage basin areas that extend into the highlands. The

© 2023 The Authors. *Sedimentology* published by John Wiley & Sons Ltd on behalf of International Association of Sedimentologists, *Sedimentology*, **71**, 319–354

13653091, 2024, 1, Downloaded from https://onlinelibrary.wiley.com/doi/10.1111/sed.13138 by Test, Wiley Online Library on [22/01/2024]. See the Terms and Conditions (https://onlinelibrary.wiley.com/terms-and-conditions) on Wiley Online Library for rules of use; OA articles are governed by the applicable Creative Commons License

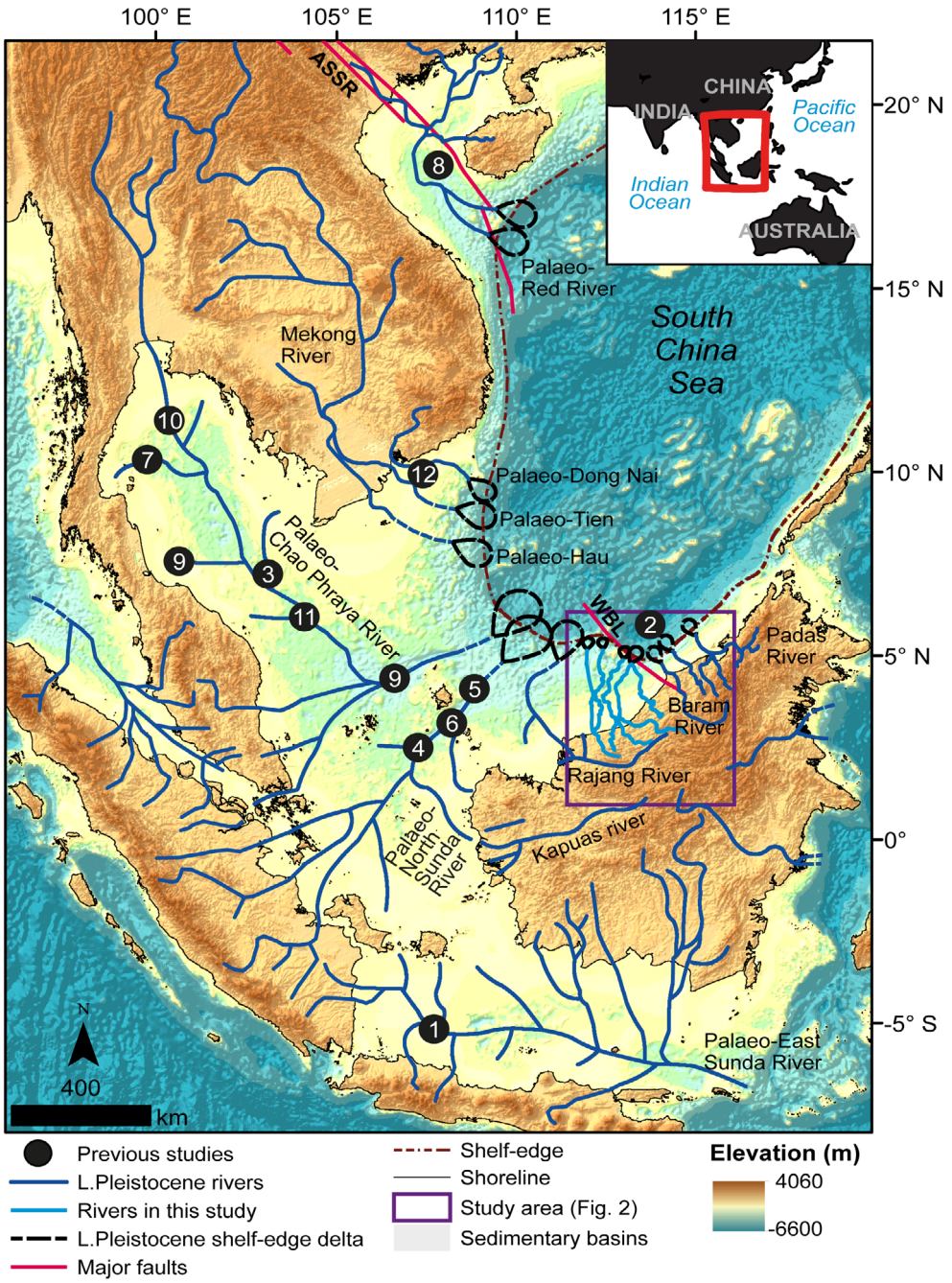


Fig. 1. Reconstruction of Late Pleistocene river networks and shelf-edge deltas along the Sunda shelf margin. The palaeo-rivers are modified from Voris (2000), Lambiase & Cullen (2013), Thanh *et al.* (2021), Wetzel *et al.* (2021). Previous Quaternary incised valleys studies are numbered on the map as follows: (1) Posamentier (2001); (2) Hiscott (2001); (3) Miall (2002); (4) Hanebuth *et al.* (2002); (5) Hanebuth *et al.* (2003); Wong *et al.* (2003); (6) Hanebuth & Stattegger (2004); (7) Samorn (2006); (8) Tanabe *et al.* (2006); Wetzel (2017); Wetzel *et al.* (2021); (9) Puchała *et al.* (2011); (10) Reijenstein *et al.* (2011); (11) Alqahtani *et al.* (2015, 2017); (12) Tjallingii *et al.* (2010); Thanh *et al.* (2021); Wetzel *et al.* (2021).

north-west Borneo shelf-edge is variable, reflecting its complex Miocene to present-day tectonic and stratigraphic history, including (i) the north-west Borneo Trough, which defines a Miocene collision zone between Borneo and the South China Sea (SCS; Hutchison, 2004), and (ii) the north-west-trending WBL, and its extension to the Red River Fault (Morley, 2002).

© 2023 The Authors. *Sedimentology* published by John Wiley & Sons Ltd on behalf of International Association of Sedimentologists, *Sedimentology*, **71**, 319–354

13653091, 2024, 1, Downloaded from https://onlinelibrary.wiley.com/doi/10.1111/sed.13138 by Test, Wiley Online Library on [22/01/2024]. See the Terms and Conditions (https://onlinelibrary.wiley.com/terms-and-conditions) on Wiley Online Library for rules of use; OA articles are governed by the applicable Creative Commons License

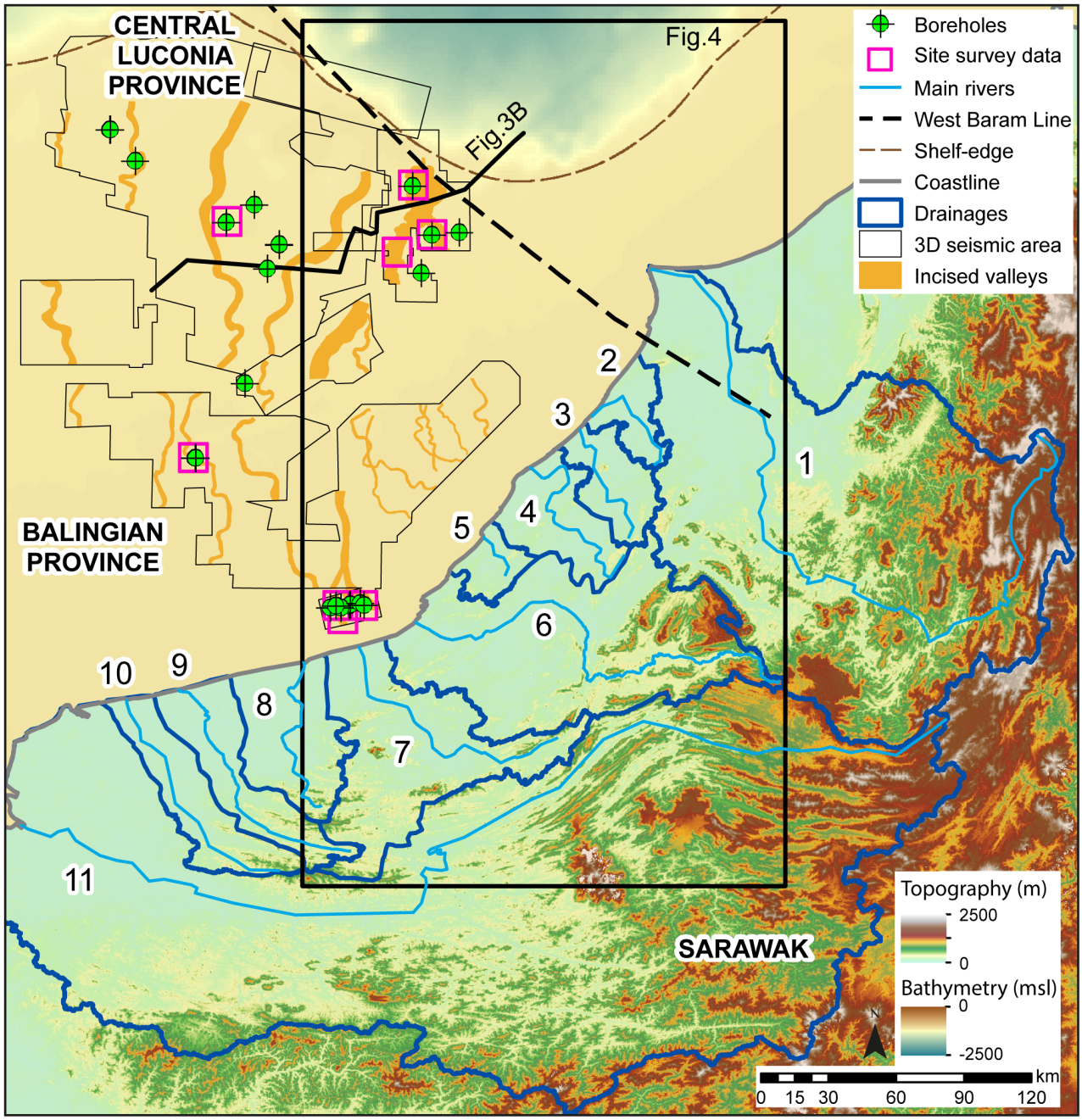


Fig. 2. Map of present-day onshore Sarawak with modern rivers (lighter blue lines) and their drainage basin areas (darker blue lines). The offshore Balingian – Central Luconia provinces comprise palaeo-valley networks mapped from three-dimensional (3D) seismic and site survey datasets. The source of data is a 30 m digital elevation model (DEM). River names: (1) Baram; (2) Sibuti; (3) Niah; (4) Suai; (5) Similajau; (6) Kemena; (7) Tatau; (8) Lemai; (9) Mukah; (10) Oya; (11) Rajang.

Tectono-stratigraphy of the eastern Central Luconia Province

The Central Luconia – Balingian area is situated on the narrow (*ca* 200 to 300 km wide) and low-gradient (*ca* 0.001°) continental shelf (Fig. 2). The northern part of the CLP adjoins the North Luconia deep-water area (−200 to −1500 m). The southern part of the Balingian Province comprises the present-day coastline, which passes landward to an elevation of *ca* 1500 m in the interior highlands.

© 2023 The Authors. *Sedimentology* published by John Wiley & Sons Ltd on behalf of International Association of Sedimentologists, *Sedimentology*, **71**, 319–354

13653091, 2024, 1, Downloaded from https://onlinelibrary.wiley.com/doi/10.1111/sed.13138 by Test, Wiley Online Library on [22/01/2024]. See the Terms and Conditions (https://onlinelibrary.wiley.com/terms-and-conditions) on Wiley Online Library for rules of use; OA articles are governed by the applicable Creative Commons License

The regional stratigraphy of the CLP comprises a thick (0.5 to 2.0 km), clastic-dominated Neogene succession, which has been divided into eight cycles (Cycles I to VIII; Fig. 3) bounded by marine flooding surfaces and/or their approximately correlative unconformities (Ho, 1978; Hageman, 1987; Lunt & Madon, 2017). Three broad stratigraphic intervals are recognized (Fig. 3): (i) Cycles I to III (Oligocene – Miocene) comprise coastal plain clastic deposits overlying strongly folded and thrusted deep-water deposits (Rajang Group), unspecified Sequence A/Pre-Cycle I deposits and/or older basement rocks; (ii) Cycles IV to V (Mid–Late Miocene) are dominated by carbonate deposits, represented by over 200 carbonate build-ups, which overlie the regionally

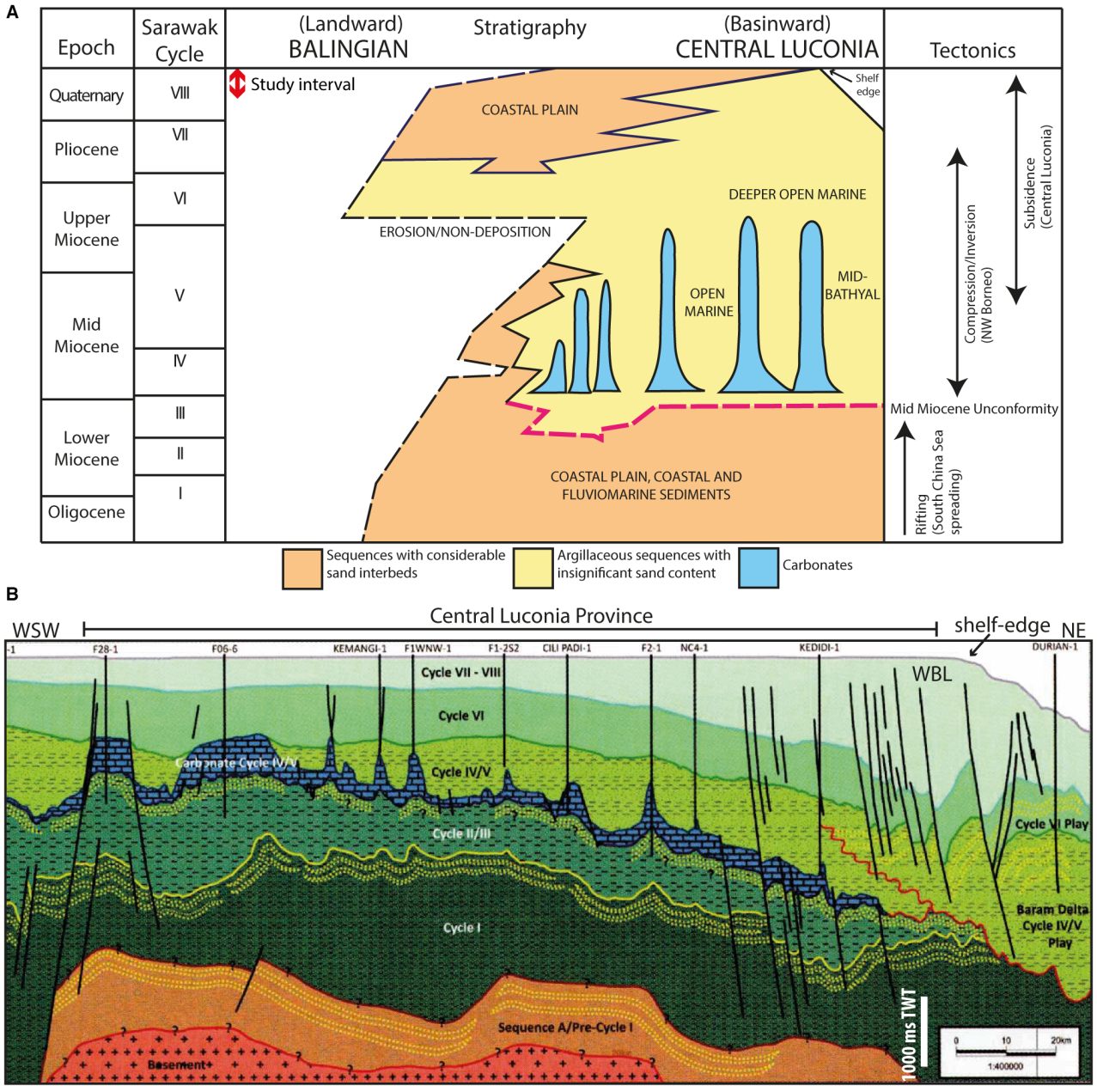


Fig. 3. (A) Tectono-stratigraphic section through the Balingian – Central Luconia provinces (modified from Ali & Abolins, 1999). (B) WSW–NE regional geoseismic section across the Central Luconia Province (CLP) towards the shelf-edge and West Baram Line (WBL; section line located on Fig. 2). This study focuses on the shallowest and youngest succession (Cycles VII–VIII), which shows a sediment wedge building out (thickening towards the north-east) to the structurally-controlled shelf-edge. Modified from Iyer (2019).

© 2023 The Authors. *Sedimentology* published by John Wiley & Sons Ltd on behalf of International Association of Sedimentologists, *Sedimentology*, **71**, 319–354

13653091, 2024, 1, Downloaded from https://onlinelibrary.wiley.com/doi/10.1111/sed.13138 by Test, Wiley Online Library on [22/01/2024]. See the Terms and Conditions (https://onlinelibrary.wiley.com/terms-and-conditions) on Wiley Online Library for rules of use; OA articles are governed by the applicable Creative Commons License

extensive Middle Miocene Unconformity (Epting, 1980; Ali & Abolins, 1999; Koša, 2015; Ting *et al.*, 2021); and (iii) Cycles VI to VIII (Late Miocene/Pliocene – Pleistocene) shallow-water clastic deposits with large-scale progradational seismic stratal geometries (Fig. 3B; Madon *et al.*, 2013; Iyer, 2019). This study is focused on the last regressive–transgressive phase, Cycle VIII (the Latest Pleistocene–Holocene).

The sedimentary sequences of the Central Luconia – Balingian provinces are influenced by both tectonics and eustasy (Hutchison, 2005; Fig. 3A). During the Late Cretaceous to Late Eocene, the South China Sea plate was subducted beneath Borneo and formed the Rajang Fold–Thrust Belt (Hutchison, 2005). The Balingian Province was subsequently dominated by compressional tectonics, episodic uplift and erosion from Eocene to Pliocene times, which resulted in a thick siliciclastic succession deposited basinward of the fold–thrust belt (Madon, 1999; Madon & Abolins, 1999; Hutchison, 2005). The Oligocene to Miocene geological history of the CLP reflects early South China Sea seafloor spreading, extensional tectonics, regional subsidence and extensive Mid–Late Miocene carbonate build-ups (Ali & Abolins, 1999; Koša, 2015). Miocene carbonate deposition was terminated by renewed influx of siliciclastic sediments in the Pliocene–Quaternary (Cycles VI–VIII), caused by uplift of the Rajang Fold–Thrust Belt (Ali & Abolins, 1999; Koša, 2015). The Mid-Miocene Unconformity marks the end of South China Sea rifting (Ali & Abolins, 1999). During the Quaternary, the WBL continued to be a long-lived tectonic lineament, which had originated in the Oligocene. It separated an extensive coastal plain area to the south-west (throughout the Central Luconia – Balingian area) from the deep-water north-west Borneo Trough to the north-east (Tan *et al.*, 1999; Cullen, 2010; Madon & Jong, 2022; Figs 2 and 4).

Quaternary geological setting of the eastern Central Luconia shelf

The Sunda Shelf is a broad, low-gradient continental shelf, located in an equatorial setting with a tropical–humid climate, high precipitation and high sediment discharge (Milliman & Syvitski, 1992). The shelf is *ca* 600 km wide in its central part (across the Malay Basin), whereas in the south-eastern part (across the Sarawak Basin) it is 300 km wide. The gentle shelf gradient (*ca* 0.001°) results in small sea-level changes having the capacity to rapidly expose or submerge the entire shelf area (Hanebuth *et al.*, 2011). At present, the Sunda Shelf is a large submerged epicontinental sea following the Holocene sea-level rise (Hanebuth *et al.*, 2003). The low-latitude setting prevented the Sunda Shelf from glaciation during the Pleistocene.

The palaeoclimatology of the area shows that the area was influenced by high humidity in the Pliocene, drier in the mid-Pleistocene, and followed by fluctuations between and wet and dry climates in the Late Pleistocene (Li *et al.*, 2013). Pollen analysis indicates that continental areas were covered by a tropical rainforest; mangroves and freshwater peats were widespread during periods of sea-level rise, especially in the late Quaternary (Bian *et al.*, 2011; Hanebuth *et al.*, 2011). In general, the last glacial maximum (LGM) climate is reported to be cooler and drier than the present-day (Morley, 2013; Wurster *et al.*, 2019).

Sea level was around 120 m below the present-day level at the LGM and thus the shoreline was located close to the present-day shelf-edge (Voris, 2000; Sathiamurthy & Voris, 2006). The broad central and more stable parts of the Sunda shelf were dissected by long rivers (*ca* >1000 km) with large drainage networks (*ca* >1 000 000 km^2), such as those of the Chao Phraya River, North Sunda River and East Sunda River (Voris, 2000; Alqahtani *et al.*, 2015). In contrast, shelfal areas closer to tectonically-active regions (for example, the north-west Borneo margin) tend to be narrower and dissected by the shorter rivers, such as the Rajang River (Voris, 2000). Several of the main modern rivers were active trunk rivers during the LGM and can be identified by subtle topographic variations across the submerged Sunda shelf, extending to the shelf-edge around the periphery of the deep-water South China Sea (Voris, 2000). Today, the modern rivers commonly occupy incised valleys and terminate at the coastline, with the river mouths reflecting drowning during the Holocene transgression.

DATASET AND METHODOLOGY

This paper focuses on the eastern CLP dataset, which consists of 3D seismic data (*ca* 4000 km^2), three high-resolution seismic sections from the site survey reports (2D seismic, pinger and boomer sections), and four geotechnical boreholes with 50 to 150 m depth (PC4, B12, B11 and NC3 boreholes; Figs 4 and 5). Firstly, the 3D seismic data was used mainly to map incised valley margins in plan-view and section view. Second, 3D seismic data were calibrated with the

© 2023 The Authors. *Sedimentology* published by John Wiley & Sons Ltd on behalf of International Association of Sedimentologists, *Sedimentology*, **71**, 319–354

13653091, 2024, 1, Downloaded from https://onlinelibrary.wiley.com/doi/10.1111/sed.13138 by Test, Wiley Online Library on [22/01/2024]. See the Terms and Conditions (https://onlinelibrary.wiley.com/terms-and-conditions) on Wiley Online Library for rules of use; OA articles are governed by the applicable Creative Commons License

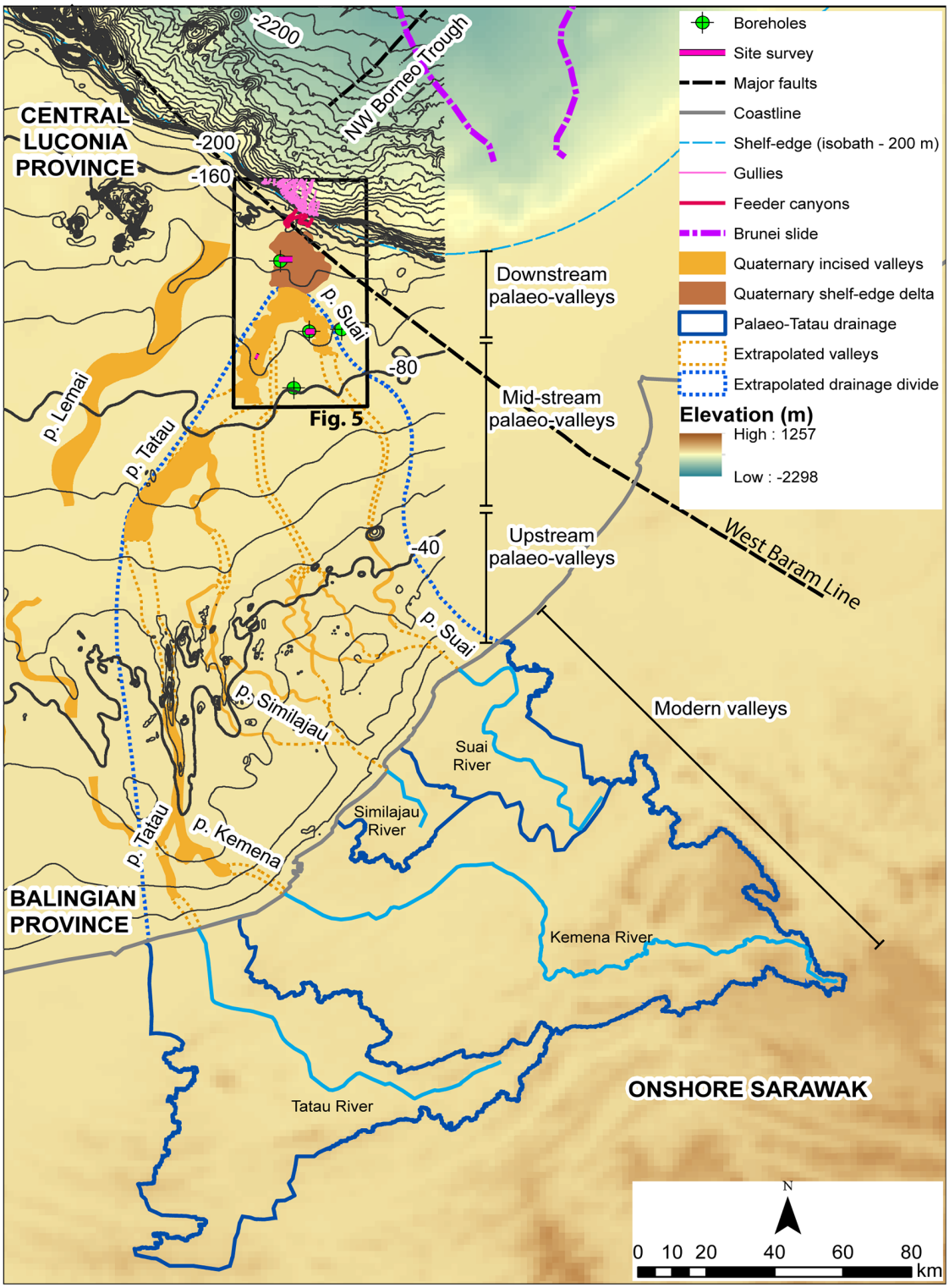


Fig. 4. Reconstruction of the complete source-to-sink, palaeo-Tatau drainage basin, which merges modern rivers (upstream) with palaeo-incised valleys in midstream (Balingian Province) and downstream areas (Central Luconia Province – CLP). Within the study area, the focus of this research has been on the eastern CLP, which comprises the Tatau incised valley, Suai incised valley and Tatau–Suai (T-S) shelf-edge delta in the downstream area. The Brunei submarine landslide is mapped from Gee *et al.* (2007).

© 2023 The Authors. *Sedimentology* published by John Wiley & Sons Ltd on behalf of International Association of Sedimentologists, *Sedimentology*, **71**, 319–354

13653091, 2024, 1, Downloaded from https://onlinelibrary.wiley.com/doi/10.1111/sed.13138 by Test, Wiley Online Library on [22/01/2024]. See the Terms and Conditions (https://onlinelibrary.wiley.com/terms-and-conditions) on Wiley Online Library for rules of use; OA articles are governed by the applicable Creative Commons License

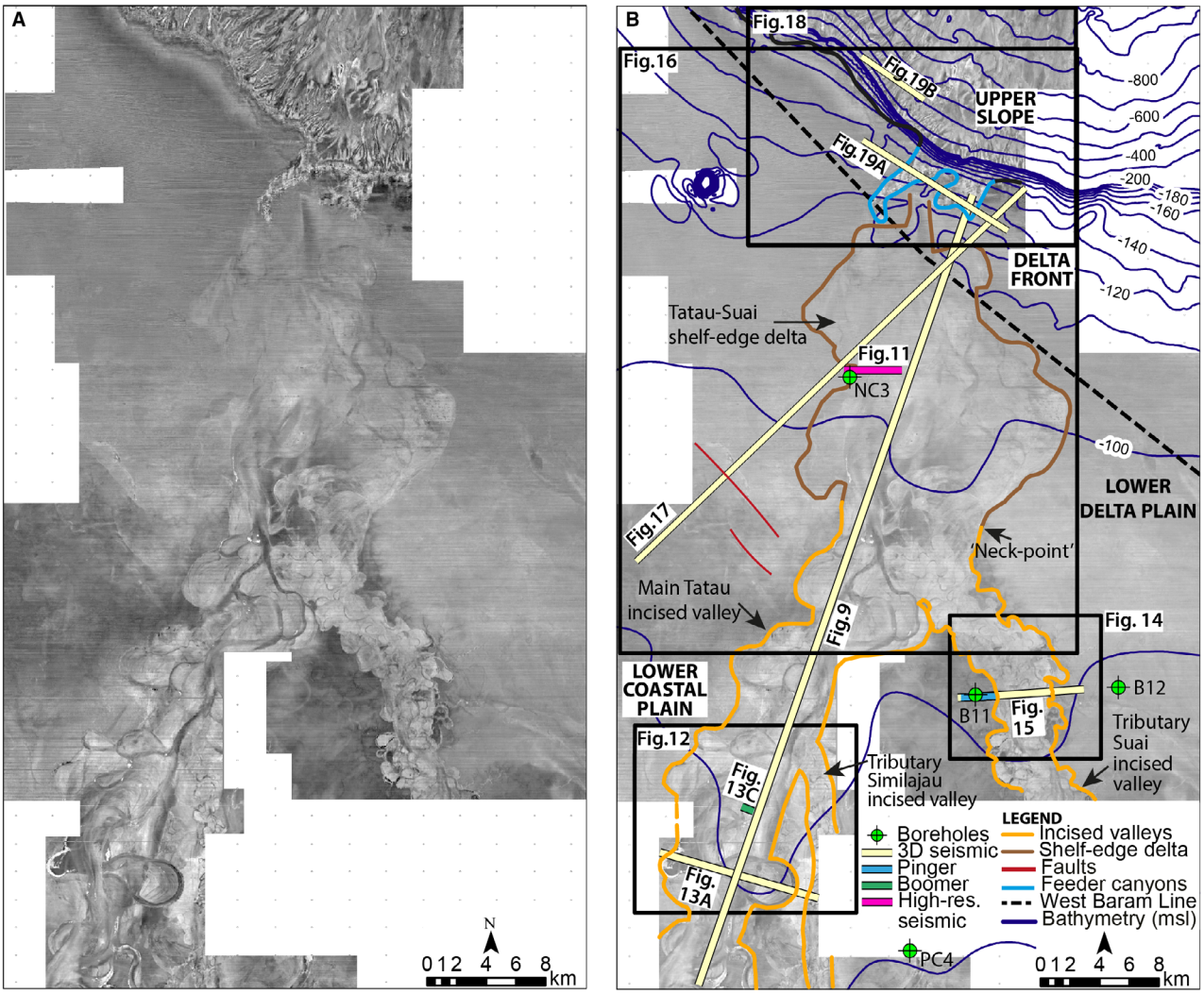


Fig. 5. The flattened time-slice map at 30 ms TWT (*ca* 24 m depth beneath the seabed) of the eastern Central Luconia Province (CLP). The grey scale colour map shows light shade of maximum seismic amplitude and dark shade of minimum seismic amplitude. (A) Uninterpreted map. (B) Interpreted incised valley and delta margin with distribution of the site survey data. The map shows Tatau, Similajau and Suai incised valleys in the landward area and transitions to the West Baram Line (WBL) fault-bounded Tatau–Suai (T-S) shelf-edge delta in the basinward area. The area is divided into lower coastal plain in the landward area, lower delta plain in the basinward area within the WBL fault zone, and delta front – upper slope in the shelf-edge to deep-water area.

high-resolution seismic sections and borehole data to identify the seismic facies and lithofacies of the: (i) Tatau incised valley fill; (ii) Suai incised valley margin and interfluve; and (iii) Tatau–Suai shelf-edge delta margin (Fig. 5). Third, the interpreted incised valleys were linked to the upstream palaeo-modern valleys.

Three-dimensional seismic reflection data

The time-migrated, 3D seismic-reflection data comprises zero-phase, reverse polarity, in which the black seismic reflection indicates minimum amplitude and red seismic reflection indicates maximum amplitude based on SEG (Society of Exploration Geophysicists). The shallow 3D seismic data have good horizontal resolution but are limited by low vertical resolution. In-line spacing is 9.5 m, cross-line spacing is 12.5 m and the data have a 2 ms vertical sampling rate. The vertical resolution of the seismic data is approximately 10 m based on the dominant frequency content of 40 Hz. A shallow sediment velocity of 1600 m/s from site survey

© 2023 The Authors. *Sedimentology* published by John Wiley & Sons Ltd on behalf of International Association of Sedimentologists, *Sedimentology*, **71**, 319–354

13653091, 2024, 1, Downloaded from https://onlinelibrary.wiley.com/doi/10.1111/sed.13138 by Test, Wiley Online Library on [22/01/2024]. See the Terms and Conditions (https://onlinelibrary.wiley.com/terms-and-conditions) on Wiley Online Library for rules of use; OA articles are governed by the applicable Creative Commons License

data (PETRONAS, 2013) was used for time-to-depth conversion to calculate depth and thickness.

The good horizontal resolution enabled the application of seismic geomorphology methods (Posamentier, 2001; Miall, 2002; Lonergan *et al.*, 2006; Zeng, 2007; Reijenstein *et al.*, 2011; Stewart *et al.*, 2013; Alqahtani *et al.*, 2015, 2017), particularly with regard to plan-view imaging and mapping of fluvial features such as incised valleys and channels. The seabed and incised valley base of the studied interval were mapped throughout the 3D seismic volume. Then, the 3D seismic volume was flattened to the seabed due to the gentle seaward dip of the seabed to map the shallowest fluvial channels observed in the flattened seismic amplitude maps. The incised valley thickness was calculated from an isopach map between the valley base and seabed. However, the relatively low vertical resolution, and the poor quality and rugose seabed reflection, limited the evaluation of cross-sectional features, such as valley/channel depth and stratigraphic architectures. This limitation was overcome in limited areas by calibrating the low-resolution 3D seismic section with the 2D high-resolution seismic data and 2D sub-bottom profile data (for example, pinger, boomer).

Site survey data

Site survey data comprise high-resolution, 2D seismic section, sub-bottom profiles and geotechnical boreholes. These data were originally acquired to determine the shallow subsurface conditions and potential hazards prior to platform installation for oil and gas production (PETRONAS, 2013). In this study, the 2D seismic data and sub-bottom profile data were calibrated with the 3D seismic data to determine seismic facies and stratigraphy. Seismic facies were calibrated with lithofacies information based on widely-spaced data from the geotechnical boreholes. This framework is used to describe the Quaternary stratigraphy, seismic geomorphology, facies and stratigraphic architecture of the Tatau valley, the Suai valley and the Tatau–Suai shelf-edge delta.

The high-resolution 2D seismic/sub-bottom profile (for example, boomer, pinger) data contain a much higher vertical resolution (0.2 to 2.0 m) than the 3D seismic data (10 m), which allows for the observation of the internal stratigraphic architecture. However, these data cover a much smaller area and have shallower penetration compared to the 3D seismic data. The 2D multichannel, high-resolution seismic has relatively high vertical resolution (2 m), deep penetration, and better seismic quality. The sub-bottom profiles (boomer, pinger, sparker) have higher vertical resolution (0.2 m) but only shallow penetration depth (*ca* 10 m deep) and low seismic quality.

Seismic facies characteristics were identified based on the combination of 3D seismic and high vertical resolution 2D seismic sections. In certain cases, the 3D seismic data prevents seismic facies interpretation because of poor vertical resolution. None of the seismic reflection characteristics observed in the 2D seismic sections are visible in the 3D seismic sections. The 2D seismic data are used to describe the seismic amplitudes, reflection geometries and continuity. These seismic facies were calibrated with the geotechnical borehole to identify the gross depositional environment.

Seismic-borehole calibration

The geotechnical boreholes were tied to the seismic data using time-depth conversion based on the site survey reports (PETRONAS, 2013). The geotechnical boreholes contain lithology information derived mainly from the grain-size analysis and cone penetration test (i.e. cone resistance, sleeve friction; Truong *et al.*, 2011; Lunne, 2012). In this study, 50 to 150 m deep boreholes were analysed based on the geotechnical properties, including cone resistance, shear strength, moisture content and plasticity index, which have been used to create sedimentary logs (Fig. 6). The cone resistance values can be used to identify stratigraphy based on sand–mud intervals, and to differentiate between clean sand, mixed sand–silt and interbedded silt and clay (Schiltz, 2020; Prins & Andresen, 2021). For example, borehole NC3 shows that sand-dominated units (LF1, LF3, LF5) are correlated with high cone resistance, whereas mud-dominated units (LF2, LF4, LF6) are correlated with low cone resistance (Fig. 6); other boreholes can be interpreted in a similar way. However, biostratigraphic analyses of borehole-derived cuttings samples were not undertaken, since these were beyond the scope of the original site investigation objectives (i.e. platform installation). Seismic facies observed in the seismic data, their associated lithofacies and borehole geotechnical properties are shown in Table 2 and discussed where relevant in the text below.

© 2023 The Authors. *Sedimentology* published by John Wiley & Sons Ltd on behalf of International Association of Sedimentologists, *Sedimentology*, **71**, 319–354

13653091, 2024, 1, Downloaded from https://onlinelibrary.wiley.com/doi/10.1111/sed.13138 by Test, Wiley Online Library on [22/01/2024]. See the Terms and Conditions (https://onlinelibrary.wiley.com/terms-and-conditions) on Wiley Online Library for rules of use; OA articles are governed by the applicable Creative Commons License

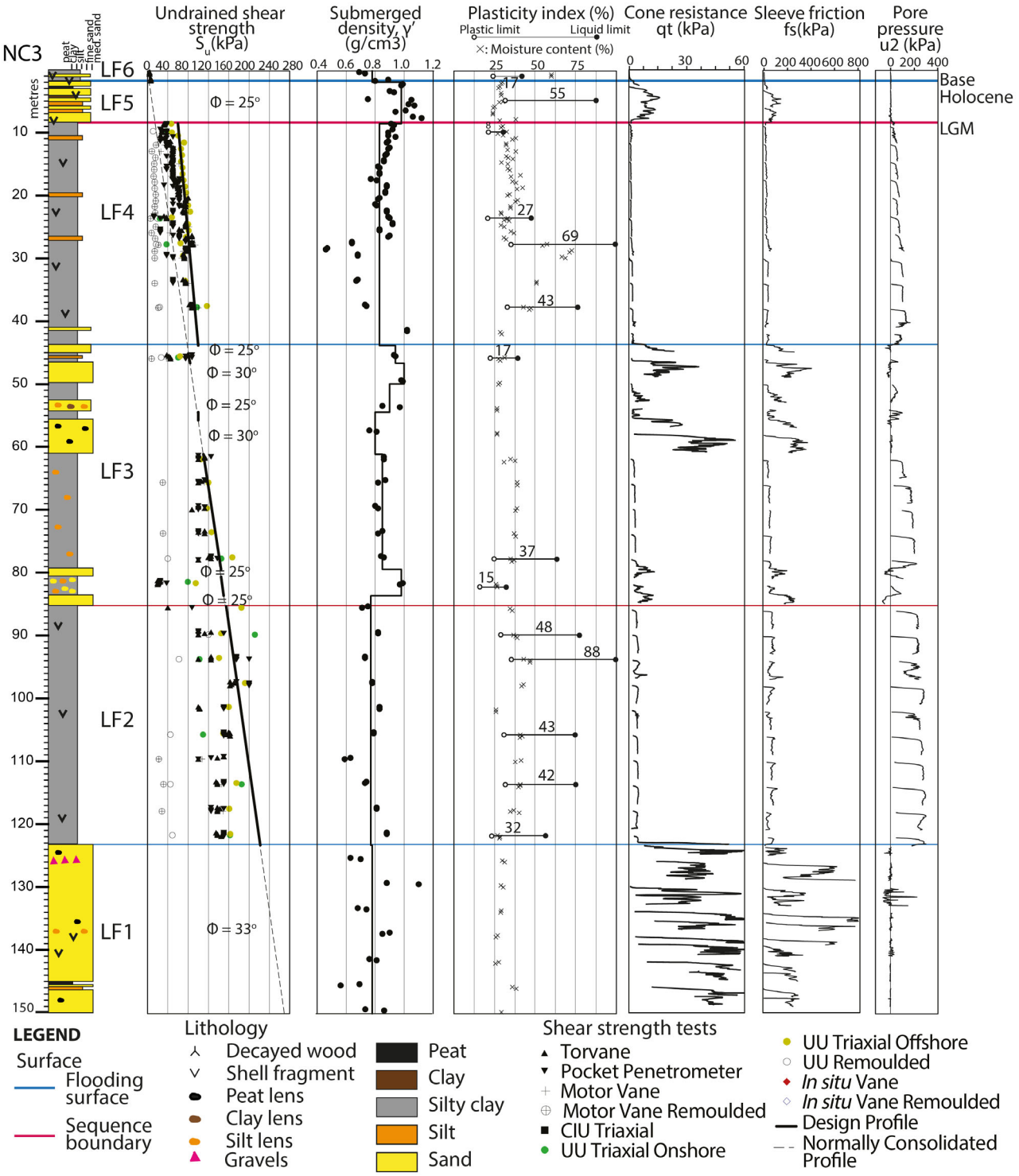


Fig. 6. 150 m deep borehole NC3 contains geotechnical properties of undrained shear strength, submerged density, plasticity index, cone resistance, sleeve friction and pore pressure values. Borehole NC3 is divided into six lithofacies (LF1–LF6). The top of the sand-dominated unit is interpreted as a flooding surface and the bottom of the respective units is interpreted as a sequence boundary.

© 2023 The Authors. *Sedimentology* published by John Wiley & Sons Ltd on behalf of International Association of Sedimentologists, *Sedimentology*, **71**, 319–354

13653091, 2024, 1, Downloaded from https://onlinelibrary.wiley.com/doi/10.1111/sed.13138 by Test, Wiley Online Library on [22/01/2024]. See the Terms and Conditions (https://onlinelibrary.wiley.com/terms-and-conditions) on Wiley Online Library for rules of use; OA articles are governed by the applicable Creative Commons License

Biostratigraphic framework

There is a comprehensive regional biostratigraphic framework for the several kilometre-thick Neogene to present-day seabed succession. This is mainly based on biostratigraphic analyses (micro-palaeontological and palynological) of hundreds of oil and gas exploration and production wells, which define a series of large-scale cycles (oldest to youngest): Cycles I to VIII (Fig. 3; e.g. Ho, 1978; Lunt & Madon, 2017). Several regionally-extensive, stratal surfaces define tectonically-influenced unconformities and/or maximum flooding surfaces based on calibration between wells (biostratigraphy, well log patterns and genetic stratigraphic) and seismic data (e.g. Levell, 1987; Cullen, 2010; Morley, 2016). These regional studies enabled the calibration of key seismic stratigraphic surfaces in the study area with their regional equivalents (Fig. 3), including the Base of the Pleistocene (Base Cycle VIII/Top Cycle VII) and near-base Pliocene (Base Cycle VII/Top Cycle VI; e.g. Koša, 2015; PETRONAS, 2019; Van Vliet & Wannier, 2023). Finer-scale calibration of the Late Pleistocene to Holocene stratigraphy was accomplished through comparison with previous studies in south-east Asia (e.g. Hiscott, 2003; Staub & Gastaldo, 2003; Hanebuth *et al.*, 2011; Twarog *et al.*, 2021). Specifically, calibration of our seismic data with Late Pleistocene–Holocene was a two-step process: (i) a sharp-based, *ca* 2 m thick veneer of fossiliferous, shallow-marine mud, which covers the seabed throughout the study area, is interpreted as Holocene sediment overlying the Base Holocene transgressive surface (for example, Fig. 6); and (ii) *ca* 10 to 30 m thick regionally-extensive and laterally-confined fluvial channels, immediately underlying the Base Holocene transgressive surface, are interpreted as incised valleys resulting from the last shelf exposure during the LGM, which follows the practice adopted by other seismic stratigraphic studies on the Sunda Shelf (e.g. Posamentier, 2001; Reijenstein *et al.*, 2011; Alqahtani *et al.*, 2015). The stratigraphy between the regionally-constrained Base Pleistocene and inferred LGM/Base Holocene cannot be dated, due to a lack of information.

DEPOSITIONAL AND STRATIGRAPHIC FRAMEWORK

The seismic geomorphological interpretations of the greater Balingian – Central Luconia area show a network of multiple, narrow to broad (*ca* 0.3 to 12 km wide), and generally northward-trending incised valleys (Fig. 4). These valleys are 200 to 350 km long and can be traced upstream to their modern, onshore equivalents to reconstruct the palaeo-drainages (Fig. 4). In the eastern part of the CLP area, which is the focus of this study, two Late Pleistocene incised valleys are represented by the present-day Tatau and Suai rivers; subsequently, termed the palaeo-Tatau and palaeo-Suai, but shortened to 'Tatau' and 'Suai' incised valleys, respectively (Fig. 4).

The Tatau and Suai incised valleys received sediments from the hinterland onshore Sarawak, which comprises folded and thrusted deep-water sandstones and mudstones of the Rajang Group (Fig. 4). In the upstream zone, the incised valleys are influenced by a partially peneplaned area in the Balingian Province area with an accretionary area to the north in the CLP area. In the downstream area (eastern CLP), the Tatau and Suai incised valleys merge, terminate at confluence zone, and form a shelf-edge delta (the Tatau–Suai, or T-S shelf-edge delta; Fig. 4). The T-S shelf-edge delta extends downstream from the valley confluence to the shelf edge, which coincides with a major tectonic lineament, the WBL. The T-S shelf-edge delta is also linked with the feeder canyons and gullies in a north-easterly-dipping slope, which trends north-west/south-east, parallel to the WBL, and extends into the deep-water north-west Borneo Trough (Fig. 4).

Seismic morphologies of the eastern Central Luconia Province

The flattened time-slice map at 30 ms two-way travel time (TWT; *ca* 24 m depth) beneath the seabed captures exceptional plan-view expression of the three genetically-linked depositional elements, namely the: (i) Tatau incised valley (a major trunk valley); (ii) Suai incised valley (a secondary tributary valley); and (iii) the Tatau–Suai shelf-edge delta (Fig. 5). The main Tatau incised valley flows north-eastward in the up-dip south-west area, whereas the tributary Suai incised valley flows north-westward in the up-dip south-east area. Another tributary incised valley (possibly Suai/Similajau) is observed in the middle area and flows northward. These tributary incised valleys merge with the main Tatau incised valleys to feed Tatau–Suai (T-S) shelf-edge delta in the northward down-dip area (Fig. 5). The

© 2023 The Authors. *Sedimentology* published by John Wiley & Sons Ltd on behalf of International Association of Sedimentologists, *Sedimentology*, **71**, 319–354

13653091, 2024, 1, Downloaded from https://onlinelibrary.wiley.com/doi/10.1111/sed.13138 by Test, Wiley Online Library on [22/01/2024]. See the Terms and Conditions (https://onlinelibrary.wiley.com/terms-and-conditions) on Wiley Online Library for rules of use; OA articles are governed by the applicable Creative Commons License

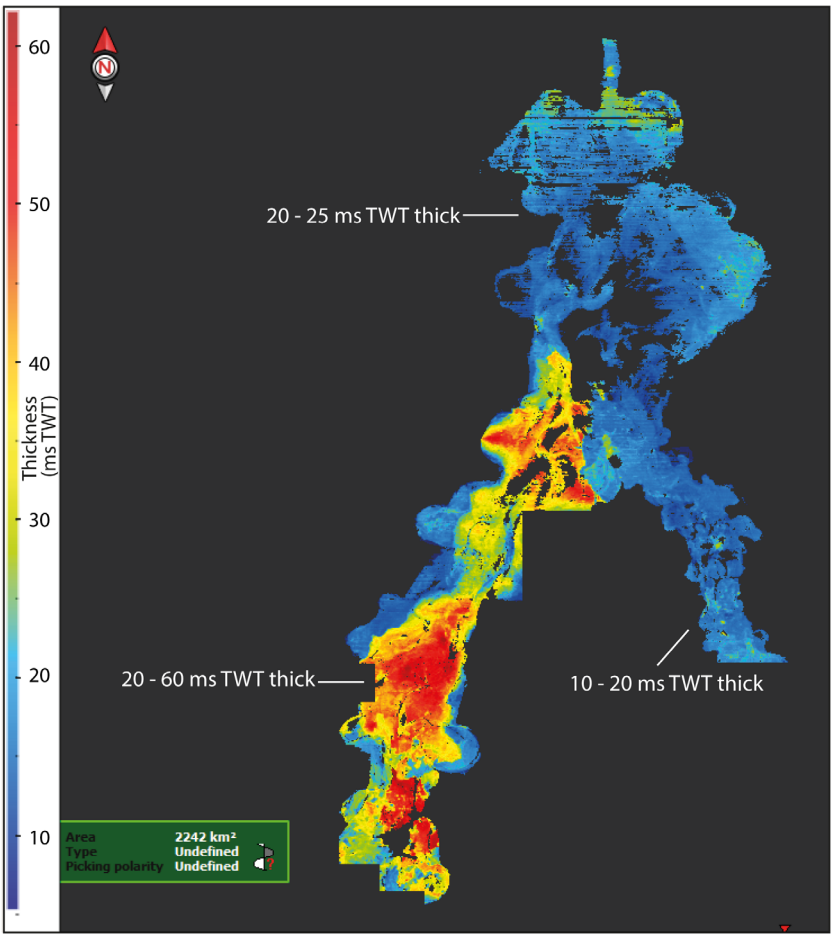


Fig. 7. Isopach map of downstream Tatau, Suai incised valleys, and Tatau–Suai (T-S) shelf edge delta generated from 3D seismic data using Paleoscan software. The Tatau incised valley fill is thicker (20 to 60 ms TWT) than the Suai valley fill (10 to 20 ms TWT thick) and T-S shelf edge delta (20 to 25 m thick).

imaging of the downstream area is more diffuse and depicts an unconfined setting of the T-S shelf-edge delta within *ca* −100 to −110 msl (Fig. 5).

The main Tatau incised valley has thicker incised valley fills (*ca* 20 to 60 ms TWT thick) compared to the tributary Suai incised valley (*ca* 10 to 20 ms TWT thick) and T-S shelf-edge delta (*ca* 20 to 25 ms TWT thick; Fig. 7; Table 1). The inner/confined part of the Tatau incised valley fill is thicker (*ca* 60 ms TWT thick) than the outer/unconfined part of the fill (*ca* 20 ms TWT thick; Fig. 7), which is defined according to the stratigraphic architecture (refer to the *Tatau incised valley* section below). The main Tatau incised valley also has broader widths than the tributary Suai incised valley (Table 1). The incised valley widths show that the Tatau and Suai incised valleys have narrower widths (*ca* 3 to 10 km wide) than the T-S shelf-edge delta (*ca* 10 to 16 km wide; Table 1).

The plan-view observation of the LGM fluvial to deltaic system is simplified as a schematic interpretation (Fig. 8), which is based on the flattened time-slice map at 30 ms TWT beneath the seabed (Fig. 5). The main Tatau incised valley is dominated by prominent scroll bars, high-sinuosity channels and larger meander-loops (*ca* 5 km wide; Fig. 8; Table 1). The tributary Suai incised valley is dominated by smaller meander-loops (*ca* 1 km wide) and abandoned channels, where the Tatau–Suai valleys merge, there are significant changes from the upstream areas (to the south) to the downstream area (to the north), and marked as a '-neck-point' transition (Fig. 8). The upstream area is dominated by the two separate valley-confined rivers, characterized by high-sinuosity, meandering channels, and the valleys merge at a confluence into a single valley within *ca* 20 km of the shelf edge. The Tatau–Suai shelf-edge delta is characterized by multiple low-sinuosity channels, and elongated sediment bars (Fig. 8). The northward area immediately adjacent to the T-S shelf-edge delta is identified

© 2023 The Authors. *Sedimentology* published by John Wiley & Sons Ltd on behalf of International Association of Sedimentologists, *Sedimentology*, **71**, 319–354

13653091, 2024, 1, Downloaded from https://onlinelibrary.wiley.com/doi/10.1111/sed.13138 by Test, Wiley Online Library on [22/01/2024]. See the Terms and Conditions (https://onlinelibrary.wiley.com/terms-and-conditions) on Wiley Online Library for rules of use; OA articles are governed by the applicable Creative Commons License

Table 1. Dimensions of the Tatau incised valley, Suai incised valley and Tatau–Suai (T-S) shelf edge delta of the east Central Luconia Province.

Area	Fluvial features	Length (m)	Width range (m)	Average width (m)	Average thickness (m)	W/D ratio	Sinuosity index
Tatau incised valley	Unconfined valley (Upper tier)	30 000	4000 ± 360–9600 ± 864	7000 ± 630	24 (140–110 ms TWT)	125	1.0
	Confined valley (Lower tier)		3000 ± 270–6600 ± 594	4600 ± 41	32 (180–140 ms TWT)		
	Young channels Meander-loop	80 000 3000	100–500	300 5000			2.1
	Old channels		200–500	350			1.2
Suai incised valley	Valley	20 000	3200 ± 288–6400 ± 576	4400 ± 392	24 (160–130 ms TWT)	130	1.0
	Young channels	20 000	70–300	180			1.5
	Meander-loop	1000		1600			
	Dendritic channels			<100	2–4	25	1.0
Tatau–Suai delta	Delta lobe	18 000	8800 ± 792–16 000 ± 1440	13 000 ± 1170	20	650	
	Young distributary channels		120 ± 33–706 ± 197	428 ± 119			1.2
	Old distributary channels		120 ± 33–279 ± 78	210 ± 58	16	14	1.3

as continental slope, which is interpreted as a rapidly deepening area beyond the continental shelf. This upper slope area is also dominated by north-east-trending headward incision at the shelf-edge, numerous very small (*ca* <100 m wide) gullies, and faulting within a north-west/south-east-trending zone of the WBL (Fig. 8). This schematic interpretation provides a basis for evaluating the seismic geomorphology of the Tatau incised valley, Suai incised valley and T-S shelf-edge delta.

Stratigraphic framework

The stratigraphic relationship between the Tatau incised valley, Suai incised valley and the Tatau–Suai shelf-edge delta is captured in an SSW–NNE-oriented (depositional dip) seismic section (Fig. 9). The lower section (*ca* 150 to 200 ms TWT) shows northward-dipping, low-angle (<0.1°) clinoforms with high amplitude and high continuity reflectors, which thickens, expands northward, and represents seismic facies one (SF1) and Units 3.1 to 3.5 (Fig. 9B; Table 2). The upper section (*ca* 100 to 150 ms TWT) shows low amplitude and low continuity reflectors (SF2, Unit 3.6), overlies a regionally-extensive erosion surface (horizon B6), which is interpreted as the LGM sequence boundary (Fig. 9; Table 2). The uppermost section (*ca* 90 to 100 ms TWT) shows continuous and high amplitude seismic reflections that drape the whole section and are interpreted as Holocene marine mudstones (SF5 and Unit 4) and overlie a regional marine flooding surface (horizon C; Fig. 9; Table 2). This stratigraphic framework is supported by the correlation of four boreholes, three from relatively more upstream locations (boreholes PC4, B12, B11) and one from a relatively further downstream location (borehole NC3; Fig. 10). Three flooding surfaces are interpreted on top of the sand-dominated units, and two sequence boundaries are interpreted at the bottom of the respective sand-dominated units (Fig. 10). From the top, Unit 4 comprises a *ca* 2 m thick mud-dominated lithofacies (LF6) with a laterally-extensive and tabular geometry; this is interpreted as the Holocene transgressive mud layer. Unit 3.6 has an irregular geometry, it thins basinward (*ca* 22 to 6 m thick) and is a sand-dominated unit with lithofacies variations (LF3, LF8, LF7, LF5; Fig. 10); this interval is interpreted as an LGM incised valley-fill succession.

The relationship between seismic facies (SF1–SF5; Fig. 9) and lithofacies (LF1–LF8; Fig. 10) is determined based on the calibration of high-

© 2023 The Authors. *Sedimentology* published by John Wiley & Sons Ltd on behalf of International Association of Sedimentologists, *Sedimentology*, **71**, 319–354

13653091, 2024, 1, Downloaded from https://onlinelibrary.wiley.com/doi/10.1111/sed.13138 by Test, Wiley Online Library on [22/01/2024]. See the Terms and Conditions (https://onlinelibrary.wiley.com/terms-and-conditions) on Wiley Online Library for rules of use; OA articles are governed by the applicable Creative Commons License

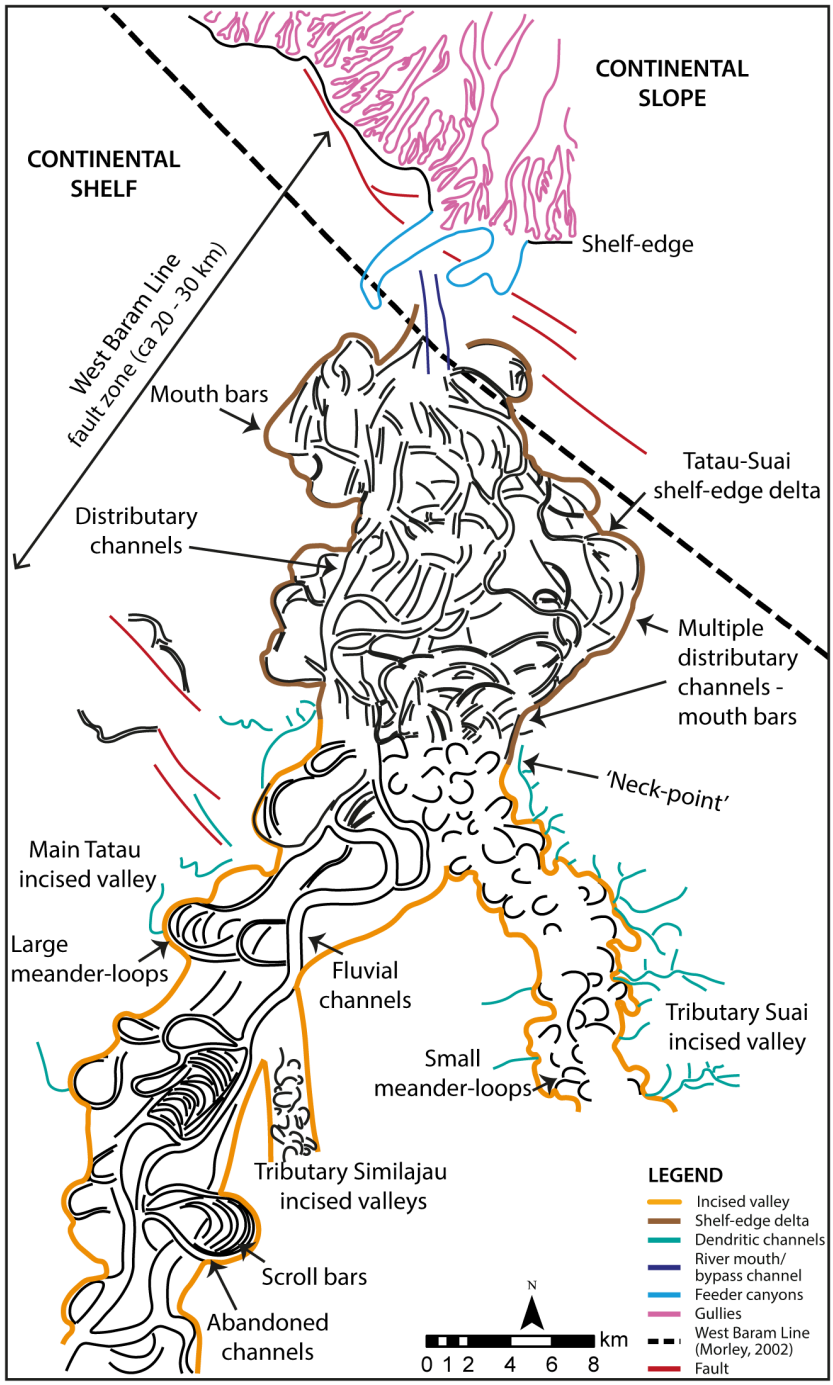


Fig. 8. Schematic interpretation of the main Tatau incised valley and tributary Suai incised valley in the southern landward area. The Tatau incised valley comprises high sinuosity and narrow fluvial channels with clear scroll bars. The tributary Suai incised valley comprises small-sized abandoned channels/meander-loops inside the valley margin and dendritic channels in the interfluve. The northern basinward area comprises Tatau–Suai (T-S) shelf-edge delta and upper slope channels. The T-S delta is dominated by mouth bars and fluvial-tidal distributary channels and terminated by the West Baram Line (WBL) at the shelf-edge.

resolution seismic and boreholes (for example, Fig. 11). SF1 is calibrated with two mud-dominated lithofacies (LF2, LF4; Fig. 11C and D, Table 2), which are characterized by their low cone resistance and sleeve friction values. LF4 is differentiated from LF2 based on its lower shear

© 2023 The Authors. *Sedimentology* published by John Wiley & Sons Ltd on behalf of International Association of Sedimentologists, *Sedimentology*, **71**, 319–354

13653091, 2024, 1, Downloaded from https://onlinelibrary.wiley.com/doi/10.1111/sed.13138 by Test, Wiley Online Library on [22/01/2024]. See the Terms and Conditions (https://onlinelibrary.wiley.com/terms-and-conditions) on Wiley Online Library for rules of use; OA articles are governed by the applicable Creative Commons License

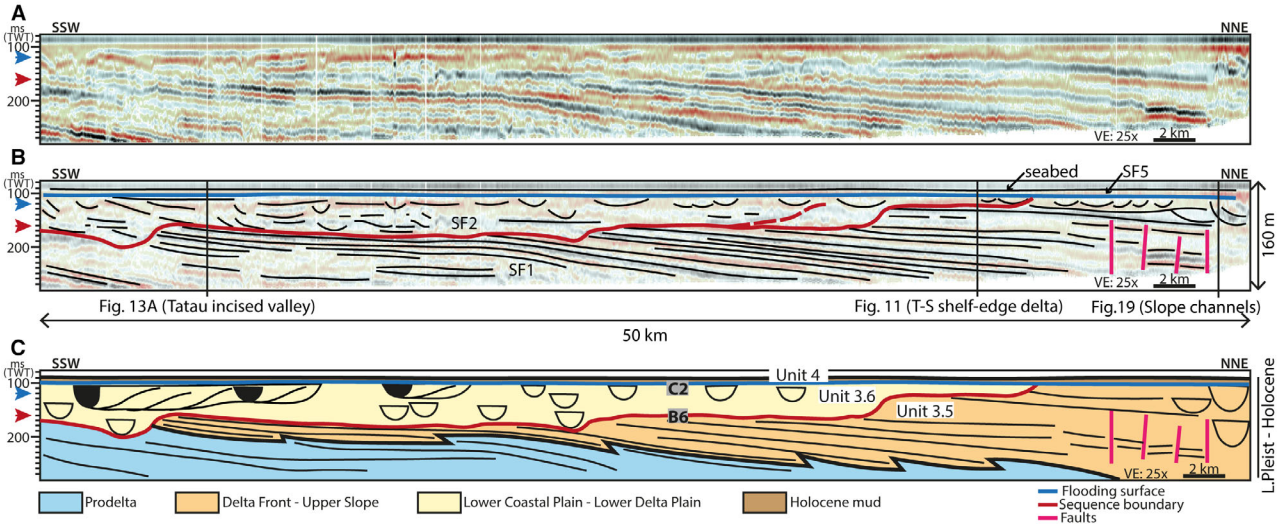


Fig. 9. SSW–NNE dip-oriented and flattened seismic section inside the Tatau incised valley, Tatau–Suai (T-S) shelf-edge delta and upper slope. Refer to Fig. 5B for seismic line location. (A) Uninterpreted seismic section. (B) The interpreted seismic section shows seismic facies SF1, SF2 and the relative position of seismic line across the incised valley. (C) Geoseismic interpretation shows the last and youngest fluvial sequence (interpreted to occur during LGM; Unit 3.6), which overlies Unit 3.5 (interpreted as delta front – upper slope), and Unit 4.2 (interpreted as Holocene mud). The seismic geomorphology of the Late Pleistocene fluvial systems is observed based on two flattened time-slice map at 70 ms TWT (red arrow) and 30 ms TWT (blue arrow) beneath the seabed.

strength (<80 kPa), higher moisture content (maximum 75%), lower plasticity index (maximum 69%) and more widespread submerged density (0.4 to 1.0 g/cm^3; Fig. 6; Table 2).

Seismic facies 2 is calibrated with three sand-dominated lithofacies (LF1, LF3, LF5), which have discontinuous geometries and variable thicknesses (Fig. 11C and D; Table 2). These lithofacies have mostly low moisture content (25 to 40%) and highly varied cone resistance, plasticity indices and submerged density (Fig. 6; Table 2). The thickest (*ca* 27 m thick) sand-body, dominated by LF1, has a consistently very high cone resistance (45 to 60 MPa) and widely-distributed submerged density (0.5 to 1.1 g/cm^3; Fig. 6; Table 2). LF3 comprises 2 to 6 m thick sand-bodies, has a much lower, serrated-shaped cone resistance (15 to 55 MPa), well-constrained submerged density (0.8 to 1.0 g/cm^3) and a low plasticity index (15 to 37%; Fig. 6; Table 2). The thinnest sand-bodies (*ca* <1 m thick) of LF5 comprise the lowest, bell-shaped cone resistance (8 to 15 MPa) and high plasticity index (55%; Fig. 6; Table 2).

Seismic facies 3 is calibrated with LF8 (Fig. 10), where borehole B12 possibly penetrates through a dendritic channel (Fig. 5) at *ca* 8 m depth and is correlated with *ca* 12 m thick sand-body (Fig. 10; Table 2). SF4 is calibrated with LF7 (Fig. 10; Table 2), where borehole B11 penetrates through the interfluve based on calibration with pinger data (refer to Suai incised valley). SF5 is calibrated with LF6 as shown in seismic-borehole NC3 calibration (Fig. 11) and present in the topmost part of all boreholes (Fig. 10; Table 2).

TATAU INCISED VALLEY

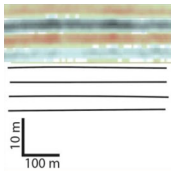
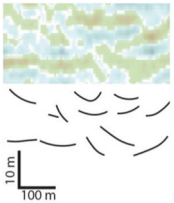
Regional context

The Tatau incised valley can be linked to the modern Tatau and Kemena rivers in onshore Sarawak (Fig. 4). The modern Tatau incised valley is *ca* 120 km long with a drainage area of *ca* 5000 km^2 (Table 1). The modern Kemena incised valley is slightly longer (220 km long) and has a larger drainage area (*ca* 8000 km^2) than the modern Tatau valley (Fig. 4; Table 1). The palaeo-Kemena valley merges with the palaeo-Tatau valley in the upstream area (Balingian Province). The total length of modern-palaeo Tatau incised valley is 340 km (Table 1). The palaeo-Tatau incised valley in the downstream area (CLP) received sediment from multiple drainage basins (Kemena, Tatau, Suai and Similajau rivers; Fig. 4). The cumulative Tatau palaeo-drainage area is estimated to be *ca* 30 000 km^2 (Table 1). Here, the Tatau incised

© 2023 The Authors. *Sedimentology* published by John Wiley & Sons Ltd on behalf of International Association of Sedimentologists, *Sedimentology*, **71**, 319–354

13653091, 2024, 1, Downloaded from https://onlinelibrary.wiley.com/doi/10.1111/sed.13138 by Test, Wiley Online Library on [22/01/2024]. See the Terms and Conditions (https://onlinelibrary.wiley.com/terms-and-conditions) on Wiley Online Library for rules of use; OA articles are governed by the applicable Creative Commons License

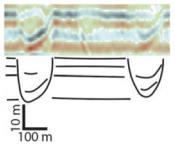
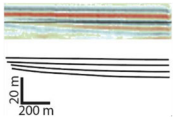
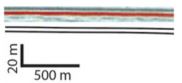
Table 2. Seismic facies (SF1–SF5) description and interpretation based on high-resolution seismic sections and boreholes.

Seismic facies (SF)	Description	Example	Lithofacies (LF)	Geotechnical properties	Interpretation
SF1	High continuity, parallel and high amplitude		LF2: 38 m thick mud-dominated unit, structureless claystone with shell fragments	Low to high shear strength (40–200 kPa), medium to very high plasticity index (32–88%), low to high moisture content (25–50%), mostly medium density (0.6–0.9 g/cm^3). Low cone resistance (8 MPa), low sleeve friction (<100 kPa) and consistently high pore pressure (300 kPa)	Floodplain (upper coastal plain)/interfluve
			LF4: 33 m thick mud-dominated unit, thin siltstone laminae and shell fragments	Very low to low shear strength (<80 kPa), low to high plasticity index (8–69%), low to very high moisture content (25–75%), high to very low density (1.0–0.5 g/cm^3). Very low cone resistance (0 MPa), very low to low sleeve friction (0 – <100 kPa), and medium low to high pore pressure (80–180 kPa)	Floodplain (lower coastal plain)/delta front/prodelta
SF2	Discontinuous, steeply dipping reflection to low-angle reflections of lateral accretion and low amplitude		LF1: 27 m thick massive sand-dominated unit with gravels, peat lens, silt lens and shell fragments	Very high shear strength (>200 kPa), mostly low moisture content (25–34%), low to high density (0.6–1.1 g/cm^3). Very high cone resistance (45–60 MPa), high to very high sleeve friction (300–800 kPa), and mostly low to occasionally high pore pressure (0–200 kPa)	Amalgamated channel complexes/ braided channels
			LF3: 21 m thick sand-dominated unit, 2 to 6 m thick fine to medium-grained sandstone bodies with peat, silt and clay intercalations and interclasts	Low to medium shear strength (<160 kPa), medium plasticity index (15–37%), low to medium high moisture content (25–40%), high to medium density (1.0 to 0.7 g/cm^3). High to low cone resistance (15–55 MPa) with serrated-shaped, high to low sleeve friction (200–400 kPa), low to high pore pressure (0–200 kPa)	Meandering fluvial channels (point bars)
			LF5: 8 m thick of interbedded fine-grained sandstone with thin siltstone, peat, and claystone laminae, gravels and shell fragments	Very low shear strength (<40 kPa), medium high plasticity index (55%), low moisture content (25–37%), medium to very high density (0.7–1.1 g/cm^3). Low cone resistance (8–15 MPa) with bell-shaped, low sleeve friction (<200 kPa) and very low pore pressure (0 kPa)	Tide-influenced channel/distributary channel/ mouth bars

© 2023 The Authors. *Sedimentology* published by John Wiley & Sons Ltd on behalf of International Association of Sedimentologists, *Sedimentology*, **71**, 319–354

13653091, 2024, 1, Downloaded from https://onlinelibrary.wiley.com/doi/10.1111/sed.1313 8 by Test, Wiley Online Library on [22/01/2024]. See the Terms and Conditions (https://onlinelibrary.wiley.com/terms-and-conditions) on Wiley Online Library for rules of use; OA articles are governed by the applicable Creative Commons License

Table 2. (continued)

Seismic facies (SF)	Description	Example	Lithofacies (LF)	Geotechnical properties	Interpretation
SF3	Localized, discontinuous, low amplitude and concave events		LF8: 12 m thick sand body with shell fragments, peat and clay intraclasts	Low shear strength (<50 kPa), low moisture content (40–50%), medium density (0.8 g/cm^3). Low cone resistance (10–17 MPa) with serrated-shaped, low sleeve friction (<120 kPa) and low pore pressure (0 kPa)	Single sinuous fluvial to tide-influenced channels/dendritic channel
SF4	High continuity, parallel lamination, high amplitude and gently dipping		LF7: 3 m thick siltstone with plant debris	Low shear strength (<80 kPa), medium density (0.8 g/cm^3), low liquidity index (0.2). Low cone resistance (<4 MPa) with bell-shaped, medium sleeve friction (<50 kPa) and low pore pressure (0 kPa)	Mangrove/swamp/estuarine
SF5	High continuity, high amplitude and structureless		LF6: 2 m thick mud-dominated unit with shell fragments	Very low shear strength (<20 kPa), low plasticity index (17%), high moisture content (60%), low density (0.7 g/cm). Very low cone resistance (0 MPa), sleeve friction (0 kPa) and pore pressure (0 kPa)	Shelf mud

© 2023 The Authors. *Sedimentology* published by John Wiley & Sons Ltd on behalf of International Association of Sedimentologists, *Sedimentology*, **71**, 319–354

13653091, 2024, 1, Downloaded from https://onlinelibrary.wiley.com/doi/10.1111/sed.13138 by Test, Wiley Online Library on [22/01/2024]. See the Terms and Conditions (https://onlinelibrary.wiley.com/terms-and-conditions) on Wiley Online Library for rules of use; OA articles are governed by the applicable Creative Commons License

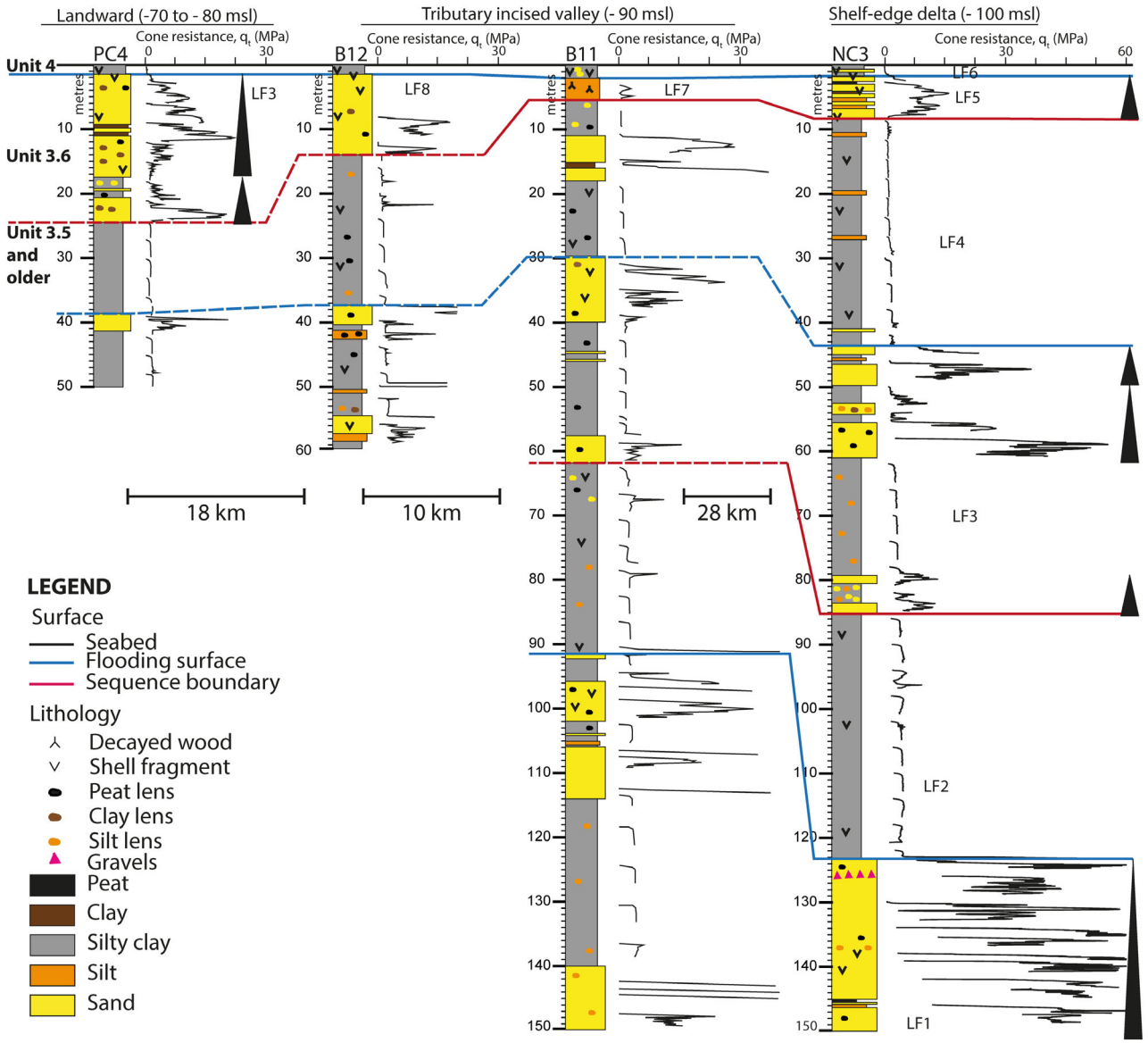


Fig. 10. Four boreholes (PC4, B12, B11 and NC3) with cone resistance values are used in this study for the stratigraphic correlation. The cone resistance shows significant change between sand-dominated and mud-dominated units. The boreholes correlation shows Unit 4 consistently presents as a 2 m thick mud-dominated unit and Unit 3.6 thins basinward from a *ca* 22 to 8 m thick sand-dominated unit.

valley is a long (*ca* 30 km length), broad (average width *ca* 7000 m wide), varying from *ca* 4000 to 10 000 m wide (Table 1), thick incised valley fill (*ca* 16 to 50 m thick; Fig. 7) and low-sinuosity (SI: 1.0) incised valley (Table 1). The seismic geomorphology of the Tatau incised valley can be observed based on two flattened time-slice maps of the lower incised valley fill (lower Unit 3.6; 70 ms TWT/*ca* 56 m depth beneath the seabed) and upper valley fill (upper Unit 3.6; 30 ms TWT/*ca* 24 m depth beneath the seabed; Fig. 12).

Plan-view morphologies

The flattened time-slice map at 70 ms TWT (*ca* 56 m depth beneath the seabed) across the lower Unit 3.6 shows mixed fluvial features of valleys and channels (Fig. 12A and B). The north-trending, short (*ca* 12 km length), broad valley (*ca* 3500 wide) dominates the eastern area and is identified based on low amplitude seismic reflections (Fig. 12B). The dendritic channels are also visible perpendicular to the

© 2023 The Authors. *Sedimentology* published by John Wiley & Sons Ltd on behalf of International Association of Sedimentologists, *Sedimentology*, **71**, 319–354

13653091, 2024, 1, Downloaded from https://onlinelibrary.wiley.com/doi/10.1111/sed.13138 by Test, Wiley Online Library on [22/01/2024]. See the Terms and Conditions (https://onlinelibrary.wiley.com/terms-and-conditions) on Wiley Online Library for rules of use; OA articles are governed by the applicable Creative Commons License

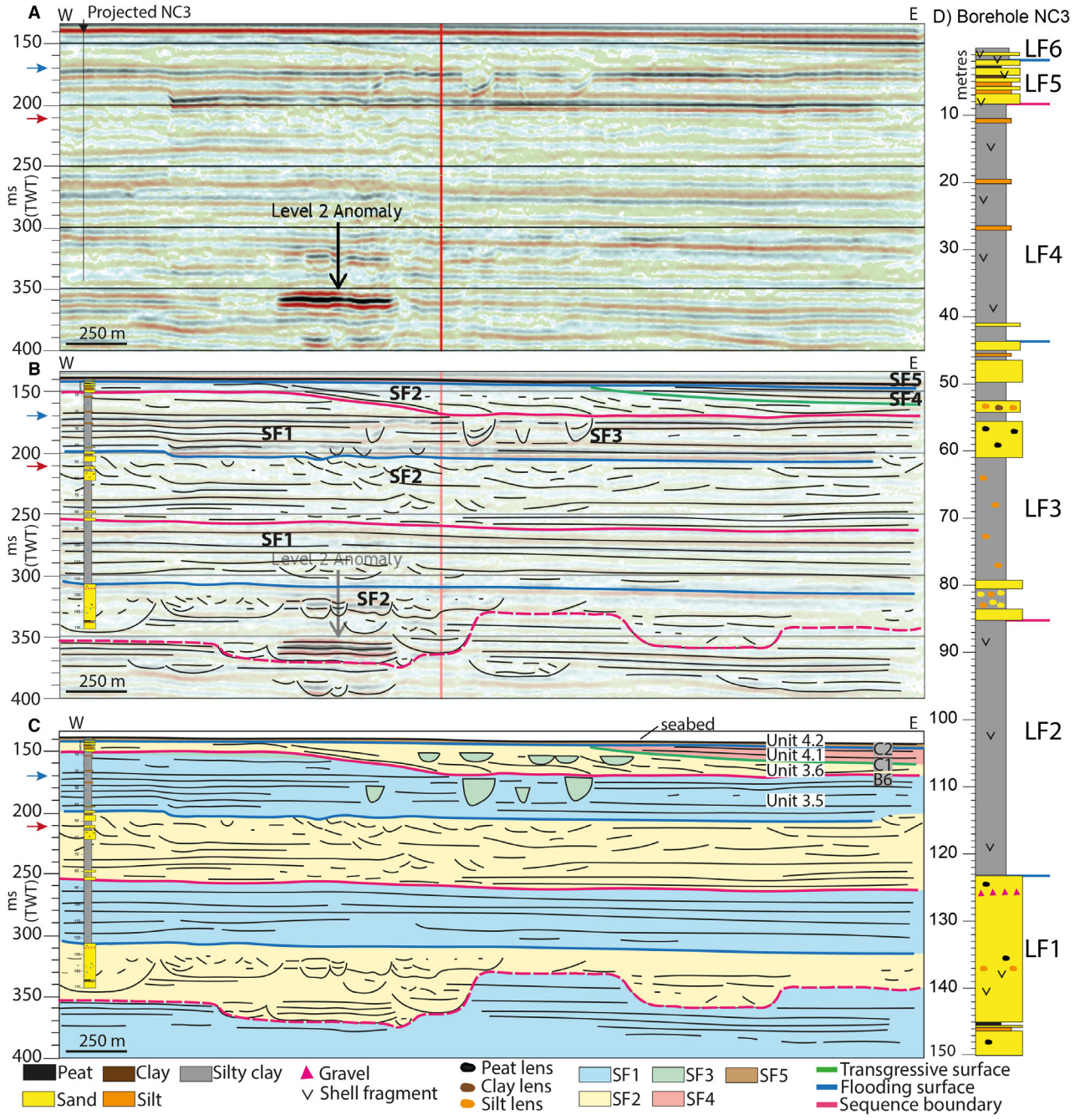


Fig. 11. The calibration of high-resolution seismic section and borehole NC3, which is located at the Tatau–Suai (T-S) shelf-edge delta margin. Refer to Fig. 5B and Fig. 16 for location. (A) Uninterpreted high-resolution seismic. (B) Interpreted high-resolution seismic identifies five seismic facies (SF1–SF5) calibrated with borehole NC3. Mud-dominated units correlate with SF1 and sand-dominated units correlate with SF2. (C) Geoseismic interpretation of the wedge-shaped T-S shelf-edge delta (Unit 3.6), which overlies Unit 3.5, is overlain by Unit 4.1 and then draped by Unit 4.2. (D) Borehole NC3 is 150 m deep and penetrates the T-S shelf-edge delta margin. The 70 ms TWT time-slice map correlates with *ca* 56 m depth beneath the seabed (red arrow) and 30 ms TWT time-slice map correlates with *ca* 24 m depth beneath the seabed (blue arrow).

valley margin. The western area is dominated by narrow (200 to 500 m wide), low sinuosity, and north to east–west trending channel segments. The eastern valley is interpreted as an old valley possibly unrelated to the Tatau incised valley, whereas the western channels

© 2023 The Authors. *Sedimentology* published by John Wiley & Sons Ltd on behalf of International Association of Sedimentologists, *Sedimentology*, **71**, 319–354

13653091, 2024, 1, Downloaded from https://onlinelibrary.wiley.com/doi/10.1111/sed.13138 by Test, Wiley Online Library on [22/01/2024]. See the Terms and Conditions (https://onlinelibrary.wiley.com/terms-and-conditions) on Wiley Online Library for rules of use; OA articles are governed by the applicable Creative Commons License

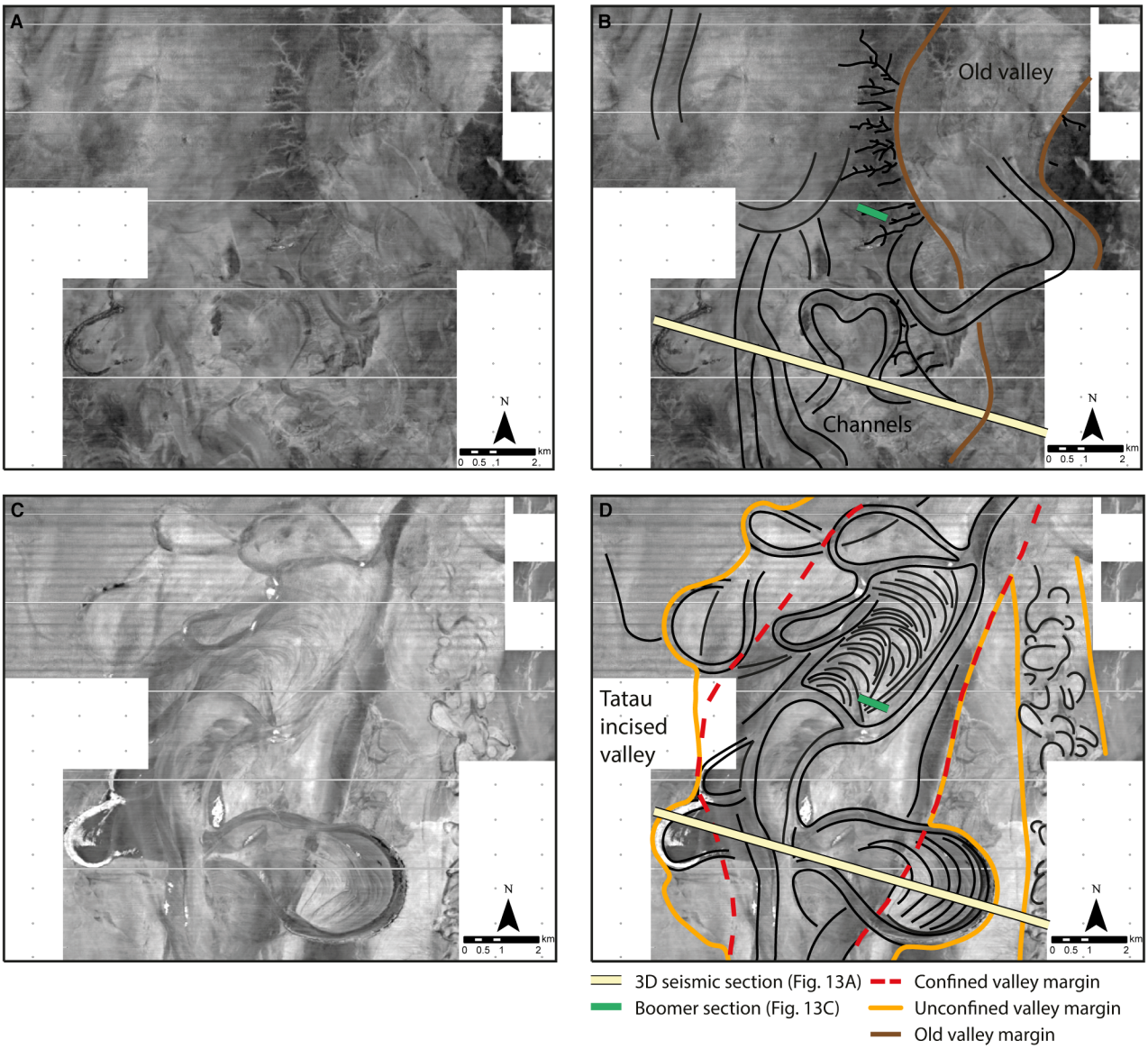


Fig. 12. The flattened time-slice map of the Tatau incised valley at: (A) and (B) 70 ms TWT beneath the seabed and across the lower Unit 3.6. The map shows broad valley and low-sinuosity channels segments. (C) and (D) The flattened time-slice map of the Tatau incised valley at 30 ms TWT beneath the seabed and across upper Unit 3.6 shows narrow and high-sinuosity channels with distinct scroll bars and point bars. Refer to Fig. 5B for the location.

are interpreted as old channels and a part of the Tatau incised valley fill.

The flattened time-slice map at 30 ms TWT (*ca* 24 m depth beneath the seabed) across the upper Unit 3.6 shows the Tatau incised valley as a very broad valley (*ca* 9000 m wide) and infilled with various fluvial features such meander-loop, scroll bars, point bar and meandering channels (Fig. 12C and D). The Tatau incised valley is also observed as an irregular and unconfined valley margin due to the presence of various sizes of meander-loops on both sides of the valley (Fig. 12D). The large-sized meander-loops (*ca* 7600 m wide by 3000 length) with clear scroll bars dominate the eastern and central part of the Tatau incised valley. The numerous small-sized meander-loops (*ca* 2500 m wide by 1600 m length) with point bars dominate the western part of the Tatau incised valley. The

© 2023 The Authors. *Sedimentology* published by John Wiley & Sons Ltd on behalf of International Association of Sedimentologists, *Sedimentology*, **71**, 319–354

13653091, 2024, 1, Downloaded from https://onlinelibrary.wiley.com/doi/10.1111/sed.13138 by Test, Wiley Online Library on [22/01/2024]. See the Terms and Conditions (https://onlinelibrary.wiley.com/terms-and-conditions) on Wiley Online Library for rules of use; OA articles are governed by the applicable Creative Commons License

meandering channels inside the valley margin are described as narrow (*ca* 300 m wide) and high-sinuosity (SI = 2.1) channels, which are commonly located at the valley edge. Another north-trending and narrower valley (*ca* 2000 m wide) is also visible on the eastern area, which is overprinted by the Tatau incised valley and is possibly related to the old valley.

The unconfined valley margin is defined by the outermost meander-loops on both sides of the Tatau incised valley (Fig. 12D). The confined valley margin is constrained within the sharp and linear valley margin on the eastern side. The western side of the confined valley margin is constrained with the small meander-loops associated with the large meander-loop in the central part of the Tatau incised valley (Fig. 12D). The unconfined Tatau incised valley shows irregular valley widths between *ca* 4000 to 9600 m for over a *ca* 30 km downstream distance (Table 1). The Tatau confined valley margin shows narrower widths within *ca* 3000 to 6600 m wide (Table 1).

Tatau incised valley facies and architecture

The lower seismic section is dominated by continuous seismic reflections (SF1) within *ca* 180 to 300 ms TWT and interrupted by discontinuous seismic reflections (SF2, SF3; Table 2; Fig. 13A). The middle seismic section is dominated by low amplitude SF2 within *ca* 140 to 180 ms TWT. The upper section comprises high amplitude seismic reflections (SF4, SF5) and interrupted SF3 within *ca* 90 to 140 ms TWT (Table 2; Fig. 13A). The boomer data covers the shallow seismic section (*ca* 125 to 165 ms TWT) within the scroll bars of the large meander-loop (labelled 'C' along part of section Fig. 13B). The boomer section differentiates the seismic facies characteristics of parallel, low-angle (*ca* <0.1°) SF4 (135 to 145 ms TWT) and structureless SF5 at 125 to 135 ms TWT (Fig. 13C and D).

The lower section is interpreted as unincised floodplain and the old valley dominates the eastern section. The middle section is identified as lower-tier Tatau incised valley (SF2), which dissects SF1 at an irregular depth within *ca* 110 to 180 ms TWT, as indicated by the confined valley base and infilled with amalgamated channel complexes (SF3; Fig. 13B). The upper section is identified as upper-tier Tatau incised valley (SF2), as indicated by the meandering channels (SF3) at both sides of the valley edge and marked as unconfined valley base. The upper Tatau incised valley also is infilled with lateral accretion (SF2), abandoned channels (SF3) and overlain with transgressive sediments (SF4), as observed in the boomer section (Fig. 13B and D). Finally, the Tatau incised valley (Unit 3.6) and interfluve (Unit 3.5) is draped with Holocene mud based on the structureless SF5 (Unit 4; Fig. 13B, D and E).

The stratigraphic architecture of the Tatau incised valley is characterized as a two-tier valley system, which comprises a confined valley base at the middle section and an unconfined valley base at the upper section (Fig. 13B and E). The lower-tier valley (lower Unit 3.6) is identified as a deeper (*ca* 50 to 90 ms TWT/*ca* 40 to 72 m depth beneath the seabed), thicker (*ca* 32 m thick), narrower (*ca* 3 to 6 km wide) and more steeply incised valley, which is infilled with narrow (350 m wide) and low sinuosity (SI: 1.2) channel segments (Fig. 12B, Table 1). The upper-tier valley (upper Unit 3.6) shows shallower (*ca* 30 to 50 ms TWT/*ca* 24 to 40 m depth beneath the seabed), thinner (*ca* 16 m thick), wider valley (*ca* 4 to 9 km wide), which is infilled with clearly imaged, narrow (300 m wide) and high sinuosity (SI: 2.1) meandering channels that extend along most of the valley lengths (Fig. 12D; Table 1). The valley is widened as the meandering channel (*ca* 200 to 500 m wide) extends beyond the confined valley margin.

SUAI INCISED VALLEY

Regional context

The Suai incised valley can be linked to the short (100 km long) and small (drainage area of *ca* 2000 km^2) modern Suai river in the onshore Sarawak (Fig. 4). The total modern-palaeo Suai valley is estimated to be *ca* 260 km long (Table 1). Here, the characteristics of the downstream Suai incised valley are identified as short (*ca* 20 km long), narrow (average width of *ca* 4400 m varying from *ca* 3000 to 6000 m wide; Table 1), thin (*ca* 10 to 20 ms TWT/8 to 16 m thick) incised valley fill (Fig. 7) and low-sinuosity (SI = 1.0) incised valley (Table 1). The Suai incised valley morphologies are mainly made from a flattened time-slice map at 30 ms TWT (*ca* 24 m depth beneath the seabed) across Unit 3.6 (Fig. 14). The Suai incised valley facies and fluvial architecture are observed based on the pinger section covering the interfluve and valley margin, and 70 m deep borehole (B11) in the interfluve (Fig. 14).

© 2023 The Authors. *Sedimentology* published by John Wiley & Sons Ltd on behalf of International Association of Sedimentologists, *Sedimentology*, **71**, 319–354

13653091, 2024, 1, Downloaded from https://onlinelibrary.wiley.com/doi/10.1111/sed.13138 by Test, Wiley Online Library on [22/01/2024]. See the Terms and Conditions (https://onlinelibrary.wiley.com/terms-and-conditions) on Wiley Online Library for rules of use; OA articles are governed by the applicable Creative Commons License

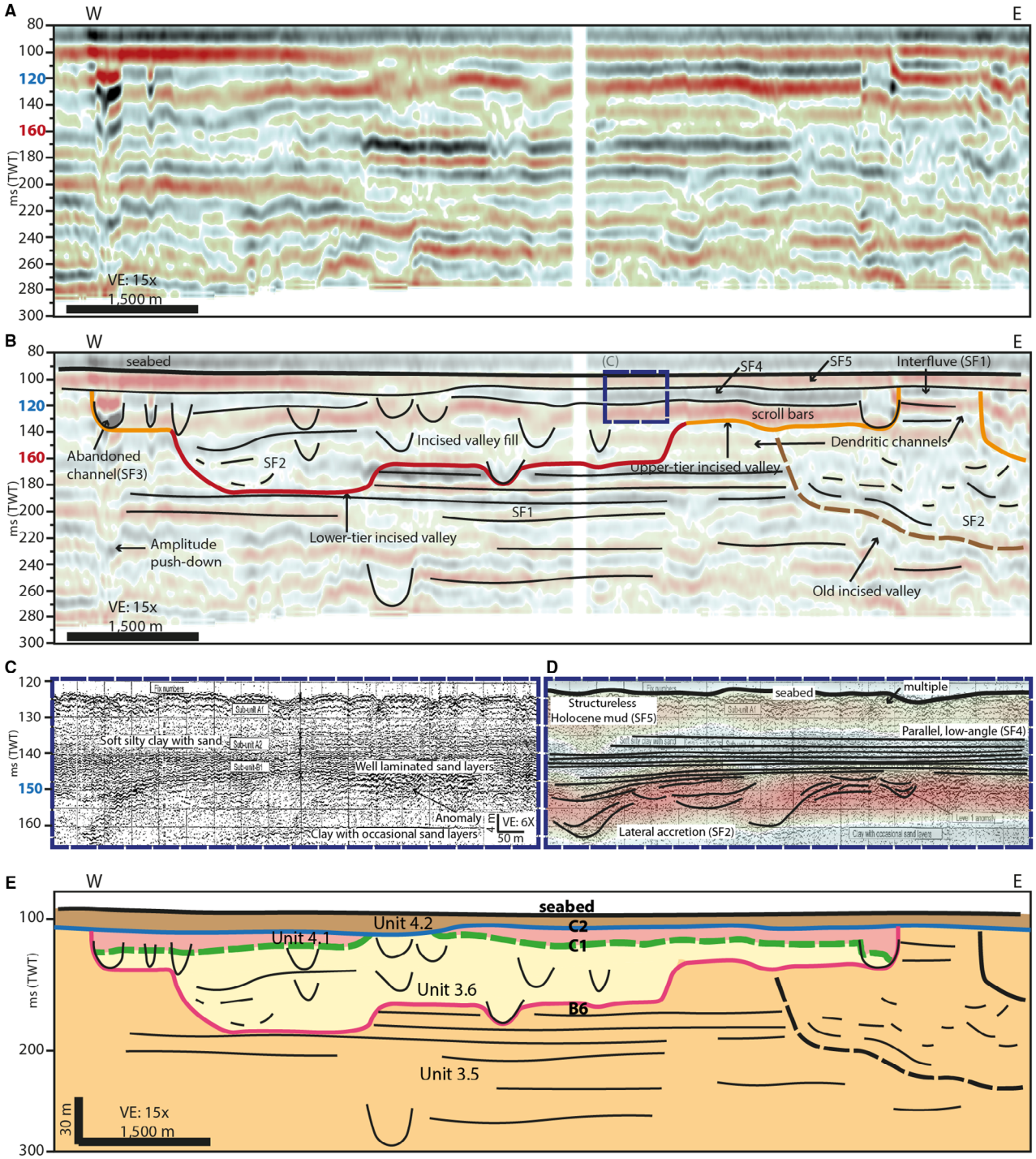


Fig. 13. The flattened seismic section of the Tatau incised valley. Refer to Fig. 12 for seismic line location. (A) Uninterpreted seismic section. (B) Interpreted seismic section shows an older incised valley fill in the lower section and the Tatau incised valley in the upper section with projected position of the boomer section (labelled as 'C'). The seismic section mainly identifies SF1 and SF2. (C) Uninterpreted boomer section located within the incised valley. (D) Interpreted boomer section identifies detailed internal fluvial morphologies as SF2, SF3 and SF4. (E) Geoseismic interpretation of the palaeo-Tatau incised valley, which comprises Unit 3.6, dissects Unit 3.5, and is infilled with Unit 4.1 and completely draped with Unit 4.2 for the whole section.

© 2023 The Authors. *Sedimentology* published by John Wiley & Sons Ltd on behalf of International Association of Sedimentologists, *Sedimentology*, **71**, 319–354

13653091, 2024, 1, Downloaded from https://onlinelibrary.wiley.com/doi/10.1111/sed.13138 by Test, Wiley Online Library on [22/01/2024]. See the Terms and Conditions (https://onlinelibrary.wiley.com/terms-and-conditions) on Wiley Online Library for rules of use; OA articles are governed by the applicable Creative Commons License

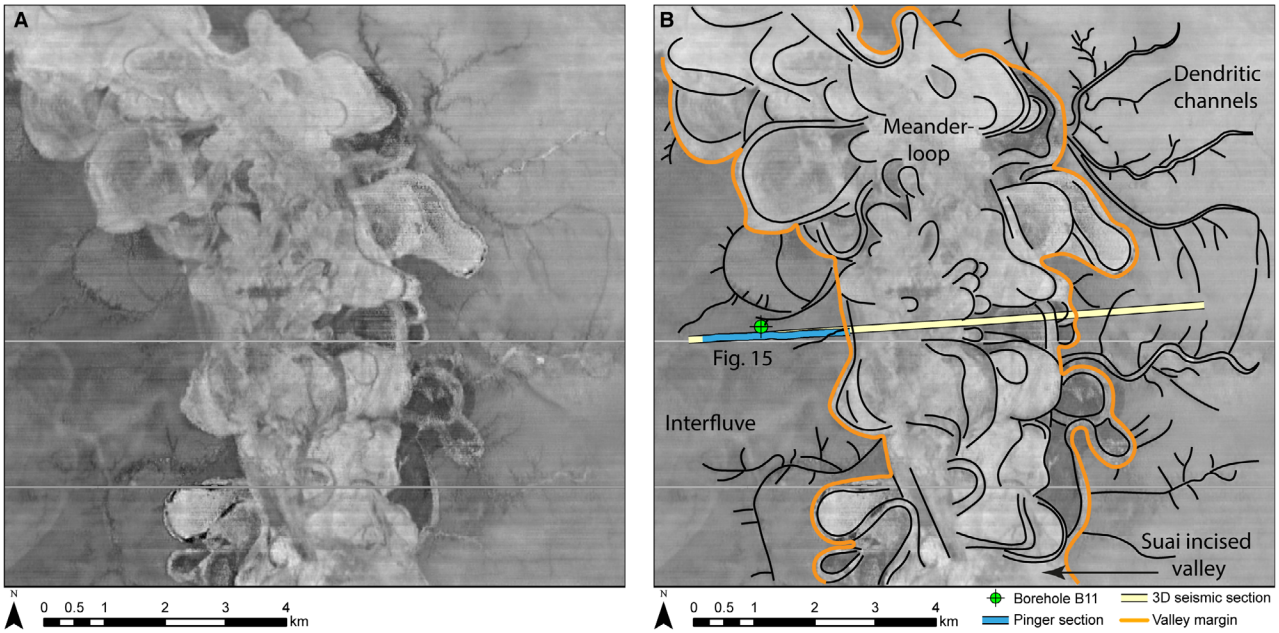


Fig. 14. A flattened time-slice map at 30 ms TWT (*ca* 24 m depth) beneath the seabed of the Suai incised valley. Refer to Fig. 5B for location. (A) Uninterpreted map. (B) Interpreted map shows an irregular incised valley margin defined by numerous dendritic channels in the interfluve and small (*ca* 1 km × 1 km) meander-loops inside the valley margins. The site survey data (pinger section, borehole B11) are located at the valley margin and interfluve area.

Plan-view morphologies

The 30 ms TWT flattened time-slice map of the Suai incised valley shows numerous small-sized meander-loops (average 1 km length by 1.6 km wide), abandoned channels, and clearly imaged dendritic channels perpendicular to the unconfined valley margin. These channels are characterized as narrower (average *ca* 180 m wide), shallower (*ca* <6 m deep), lower width/depth aspect ratio (<30) and very sinuous (SI: 1.5) compared to the Suai incised valley (Fig. 14). The Suai incised valley produces variable valley widths, fluctuating between *ca* 3200 ± 144 m and 6400 ± 264 m over a downstream length of *ca* 20 km (Table 1). The irregular and fluctuating valley widths are caused by several meander-loops and abandoned channels that extend beyond the confined valley margins.

Suai incised valley facies and architecture

The seismic section across the Suai incised valley shows that continuous SF1 dominates the lower section (*ca* 160 to 200 ms TWT) and discontinuous SF2 and SF3 dominates the central part of the section (*ca* 120 to 160 ms TWT; Fig. 15A). The Suai incised valley is recognized based on distinct SF2, which dissects SF1, and the sharp valley margin and valley base within 130 to 160 ms TWT (Fig. 15B). SF2 comprises high seismic variation between the eastern and western valley margin. High seismic amplitude and high continuity SF2 dominates the eastern part of the valley and SF3 marks the eastern valley edge (Fig. 15B).

Low seismic amplitude and low continuity SF2 and SF3 dominates the western part of the valley (Fig. 15B). The pinger section at the western valley margin also shows SF2 as steeply dipping seismic reflections that terminate at the shallow section (*ca* 125 ms TWT; Fig. 15C and D). In the interfluve, the pinger section is dominated by shallow SF3 (*ca* 4 m deep), which overlie SF1 in the lower section (*ca* 125 to 140 ms TWT). The uppermost pinger section (*ca* 120 to 125 ms TWT) comprises structureless seismic reflections (SF5) and is calibrated with *ca* 2 m thick mudstone with shell fragments and sand intraclasts (Fig. 15D).

The section below the Suai incised valley is interpreted as floodplain and interfluve (Unit 3.5) based on the mud-dominated unit (Fig. 15D and E). The upper section is identified as the Suai incised valley (Unit 3.6; Fig. 15E), which is

© 2023 The Authors. *Sedimentology* published by John Wiley & Sons Ltd on behalf of International Association of Sedimentologists, *Sedimentology*, **71**, 319–354

13653091, 2024, 1, Downloaded from https://onlinelibrary.wiley.com/doi/10.1111/sed.13138 by Test, Wiley Online Library on [22/01/2024]. See the Terms and Conditions (https://onlinelibrary.wiley.com/terms-and-conditions) on Wiley Online Library for rules of use; OA articles are governed by the applicable Creative Commons License

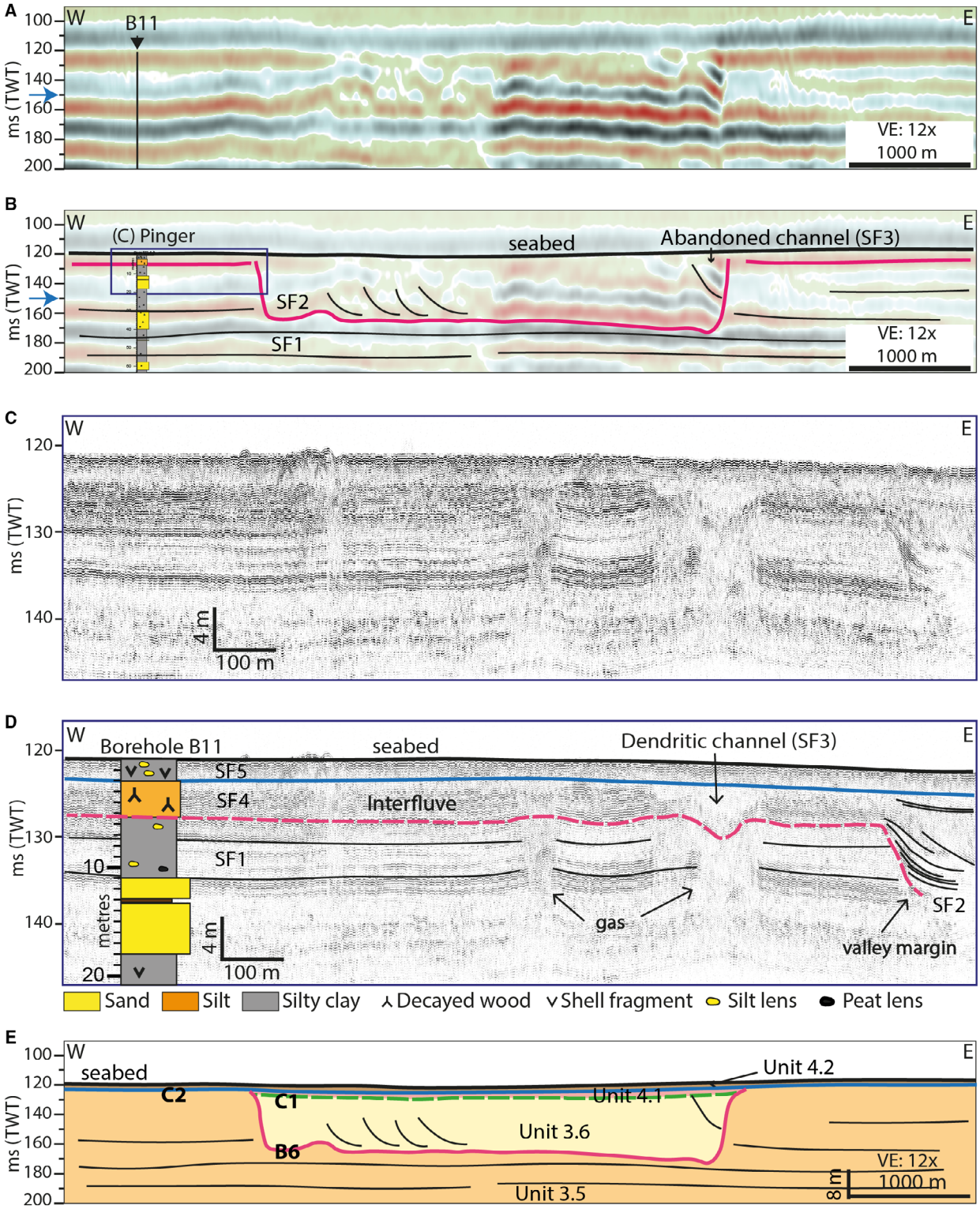


Fig. 15. (A) and (B) Uninterpreted and interpreted seismic section of the Suai incised valley differentiates SF1 and SF2 with calibrated site survey data in the western valley margin. (C) and (D) Uninterpreted and interpreted pinger section within the interfluve and the Suai valley margin identifies steeply-dipping seismic reflections truncated at the valley margin (SF2) and dendritic channels (SF3) in the interfluve. (E) Geoseismic interpretation of the Suai incised valley comprises Unit 3.6 dissects Unit 3.5 and is draped by *ca* 2 m thick Unit 4.2.

© 2023 The Authors. *Sedimentology* published by John Wiley & Sons Ltd on behalf of International Association of Sedimentologists, *Sedimentology*, **71**, 319–354

13653091, 2024, 1, Downloaded from https://onlinelibrary.wiley.com/doi/10.1111/sed.13138 by Test, Wiley Online Library on [22/01/2024]. See the Terms and Conditions (https://onlinelibrary.wiley.com/terms-and-conditions) on Wiley Online Library for rules of use; OA articles are governed by the applicable Creative Commons License

infilled with abandoned channels in the eastern valley margin and numerous small meander-loops in the western margin as observed in the plan-view (Fig. 14). The uppermost section is interpreted as Holocene mudstone based on structureless seismic facies and mud-dominated unit (SF5). The shallow (*ca* 4 m deep) and narrow (*ca* <50 m wide) channels in the interfluve are identified as dendritic channels, which are oriented perpendicular to the western valley margin (Figs 14 and 15E).

The stratigraphic architecture of the Suai incised valley is characterized as a single-tier valley system (Unit 3.6) and a sharp valley base (horizon B6), which dissects Unit 3.5 and is overlain with Unit 4.2 (Fig. 15E). The single-tier valley (Unit 3.6) is shallow (*ca* 10 ms TWT/*ca* 8 m depth beneath the seabed), thin (*ca* 24 m thick), narrow (*ca* 4 km wide), and is infilled with abandoned channels and small meander-loops (*ca* 1 km wide; Figs 14 and 15E; Table 1). Towards the downstream area, the Suai incised valley merges with the Tatau incised valley and feeds Tatau–Suai shelf-edge delta (Fig. 8). The merger is observed as a valley confluence (Fig. 8) with significant lateral width changes from *ca* 8 km wide to 12 km wide.

TATAU–SUAI SHELF-EDGE DELTA

Regional context

The Tatau–Suai (T-S) shelf-edge delta is located immediately downstream of the Tatau–Suai valley confluence with an oval shape (*ca* 18 km length, *ca* 13 km wide) within the delta plain – delta front area (Fig. 8). The T-S shelf edge delta is recognized based on the significant fluvio-deltaic transition from narrow (*ca* 300 m wide), high-sinuosity channels and numerous meander-loops in the incised valleys (southward area) to wider (*ca* 1000 m wide), low-sinuosity distributary channels and lobate-shaped mouth bars in the deltaic setting (northward area; Fig. 8; Table 1). This fluvio-deltaic transition occurs at a 'neck-point' *ca* 20 km from the shelf-edge and corresponds to the north-west/south-east WBL fault zone (Fig. 8). The T-S shelf-edge delta also is marked by significant width increase from *ca* 4000 m wide in the upstream (T-S valleys) to 8000 to 12 000 m wide at *ca* 30 km downstream distance (Table 1). The down-dip part of the T-S shelf-edge delta is dominated by the north-west-trending West Baram Line and active river mouth, which transports sediments to the deep-water system through feeder canyons and gullies on the continental slope (Figs 8 and 16).

Tatau–Suai shelf-edge delta morphologies and facies

Plan-view morphologies

The flattened time-slice map at 70 ms TWT (*ca* 56 m depth beneath the seabed) across Unit 3.5 (Fig. 16A and B) shows dominant north-west/south-east lineaments with a mixture of fluvial and deltaic features widely distributed in the southward and northward areas. The southward area is dominated by lobate to arcuate features and linear to sinuous channel segments, whereas the northward area is dominated by north-west-trending linear features, north-east-trending headward incision and high amplitude seismic reflections (Fig. 16A). The north-west-trending linear features are interpreted as fault segments associated with the WBL based on their similar orientations (Fig. 16B). Narrow to wide (*ca* 100 to 500 m wide) channel segments are interpreted as fluvial to distributary channels. The lobate-arcuate features are interpreted as fluvio-deltaic sediment bars and slumps. The sediment bars are identified based on the presence of channel segments, whereas slumps are interpreted based on the presence of north-west-trending faults perpendicular to the arcuate features mostly in the upper slope area (Fig. 16B).

The flattened time-slice map at 30 ms TWT (*ca* 24 m depth beneath the seabed) across Unit 3.6 (Fig. 16C and D) shows various channel morphologies from the southward to northward areas. The southward area is dominated by narrow-to-wide high sinuosity channels and north-west-trending linear features (Fig. 16C). The central area shows diffuse images of narrow-to-wide low sinuosity channels and featureless arcuate to elongated bars, whereas the northward area is dominated by high amplitude north-east-trending channels (Fig. 16C). In the southward area, the north-east-trending, wide (*ca* 500 m wide), high sinuosity channels are associated with the Tatau incised valley, whereas the north-west-trending, narrow (*ca* 100 m wide), high-sinuosity channels are associated with the Suai incised valley (Fig. 16D). Beyond the 'neck-point', these fluvial channels are no longer visible and become narrow-to-wide (*ca* 100 to 800 m wide), low-sinuosity

© 2023 The Authors. *Sedimentology* published by John Wiley & Sons Ltd on behalf of International Association of Sedimentologists, *Sedimentology*, **71**, 319–354

13653091, 2024, 1, Downloaded from https://onlinelibrary.wiley.com/doi/10.1111/sed.13138 by Test, Wiley Online Library on [22/01/2024]. See the Terms and Conditions (https://onlinelibrary.wiley.com/terms-and-conditions) on Wiley Online Library for rules of use; OA articles are governed by the applicable Creative Commons License

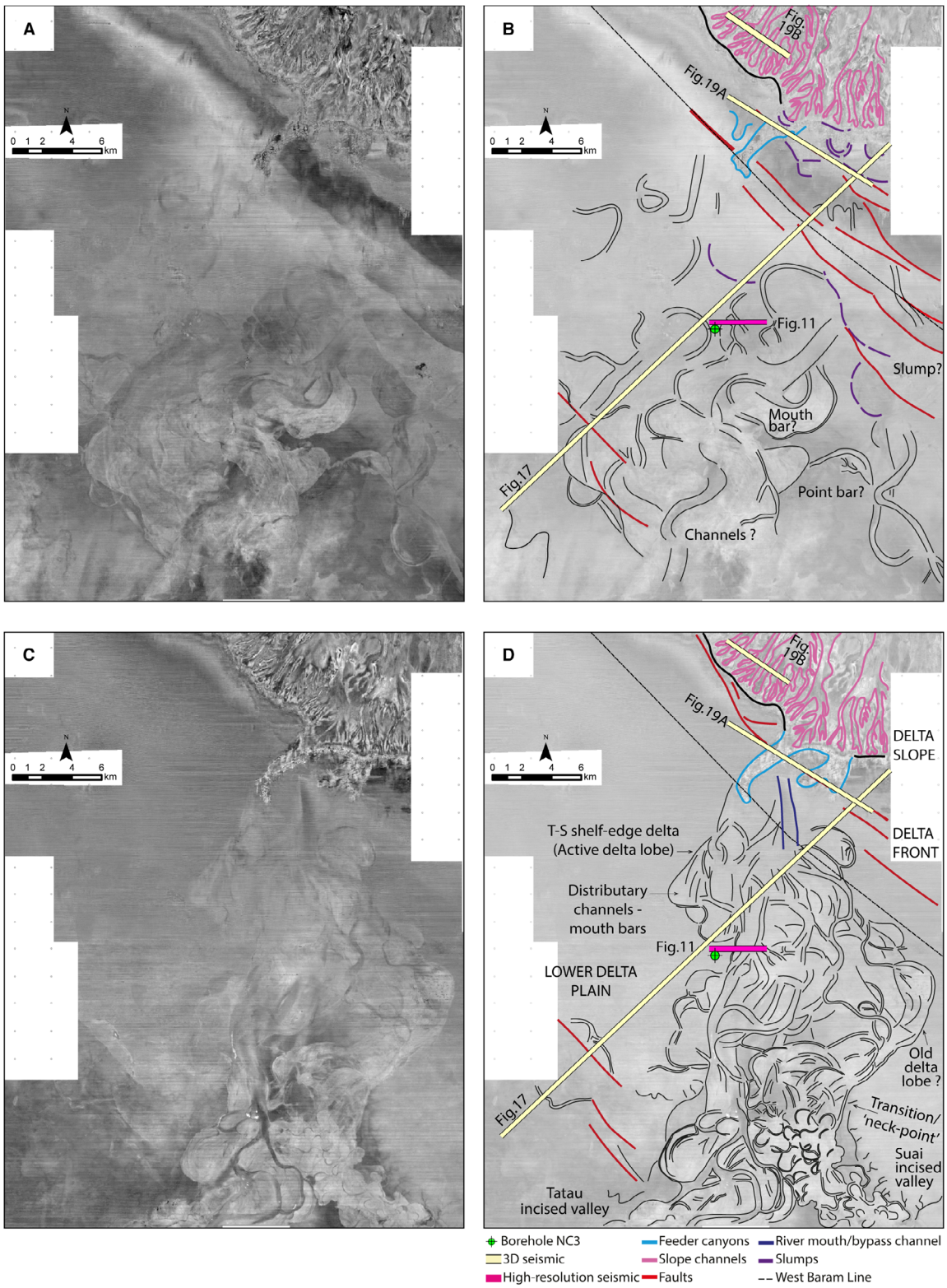


Fig. 16. Two flattened time slices of the Tatau–Suai (T-S) shelf edge delta. (A) and (B) Flattened time-slice map at 70 ms TWT beneath the seabed, which shows a mix of fluvial and deltaic features. (C) and (D) Flattened time-slice map at 30 ms TWT beneath the seabed, which shows high sinuosity channels within the Tatau and Suai incised valleys in the southern landward area and low sinuosity, lobate – elongated features in the northern basinward area. The transition from incised valleys to the shelf-edge delta is marked as 'neck-point' located in Fig. 8.

© 2023 The Authors. *Sedimentology* published by John Wiley & Sons Ltd on behalf of International Association of Sedimentologists, *Sedimentology*, **71**, 319–354

13653091, 2024, 1, Downloaded from https://onlinelibrary.wiley.com/doi/10.1111/sed.13138 by Test, Wiley Online Library on [22/01/2024]. See the Terms and Conditions (https://onlinelibrary.wiley.com/terms-and-conditions) on Wiley Online Library for rules of use; OA articles are governed by the applicable Creative Commons License

distributary channels and coalesced, multiple mouth bars dominate the central area, which are associated with the Tatau–Suai shelf-edge delta (Fig. 16D). Overall, the southward to central areas show fluvial channels confined within the Tatau and Suai incised valleys in the up-dip area and transitioned to unconfined, multiple distributary channels – mouth bars in the down-dip area. Thus, the T-S shelf-edge delta comprises unconfined and multiple distributary channels – mouth bars, which are distributed laterally and prograded northward until the WBL (Fig. 16D).

Tatau–Suai shelf-edge delta facies and architecture

The strike-oriented, high-resolution seismic section of the T-S shelf-edge delta margin shows alternated SF1 and SF2 in the lower section (*ca* 200 to 400 ms TWT) and various seismic facies in the upper section (160 to 200 ms TWT; Fig. 11A). The upper section comprises continuous and high amplitude SF1, interrupted by localized SF3 within *ca* 170 to 200 ms TWT, overlain by steeply-dipping and low amplitude SF2 in the west side, wedge-shaped SF4 in the east side within 150 to 170 ms TWT, and draped by continuous SF5 at *ca* 160 ms TWT (Fig. 11A).

The interval of seismic facies SF1 are interpreted as coastal plain to delta plain deposits based on correlation with *ca* 30 m thick mud-dominated unit with shell fragments (Fig. 11C). The interval of seismic facies SF2 are interpreted as fluvial deposits based on thicker sand-bodies (*ca* 4 to 30 m thick; Fig. 11C). The uppermost interval of SF2 (Unit 3.6) is interpreted as 8 to 24 m thick mouth bars with fluvio-tidal distributary channels based on lateral accretion, and thin sand-bodies (<1 m thick) with shell fragments and a peat layer (Fig. 11C). SF3 is interpreted as distributary channels within Unit 3.5. SF4 is interpreted as transgressive deposits (estuarine to mangrove deposits) based on its *ca* <8 m thick wedge-shaped geometry (Unit 4.1), which onlaps the mouth bar deposits (Unit 3.6). SF5 is interpreted as Holocene mud (Unit 4.2) based on its correlation to a 2 m thick mud-dominated unit with shell fragments.

Based on this, the authors interpret the youngest interval of SF2 (Unit 3.6) as the T-S shelf-edge delta margin, which formed during the Latest Pleistocene. It overlies the Pleistocene deposits and is overlain by transgressive deposits during the initial sea-level rise and, finally, draped by the Holocene mud during the complete submergence (Fig. 11C). The interpretation of the T-S shelf-edge architecture also highlights thin deltaic deposits (*ca* 16 to 24 m thick; Figs 7 and 11C) and thin sand-bodies (*ca* 1 m thick), which possibly indicate that the sediments have been bypassed to the upper slope (Fig. 16D).

The sediment bypass from the T-S shelf-edge delta to the upper slope can be observed based on the presence of river mouths and feeder canyons at the tectonically influenced shelf-edge (Fig. 16D). Most of the distributary channels – mouth bars are constrained within the WBL but several river mouths extend northward towards the irregular shelf-edge (Fig. 16D). The flattened time-slice map at 30 ms TWT also suggests that the T-S shelf-edge delta is controlled by the WBL, as the delta occurs immediately within the north-west-trending fault segments in the southward area (indicated by 'neck-point') and ceased towards the shelf-edge.

The relationship between the T-S shelf-edge delta and the WBL fault zone is observed on the seismic section perpendicular to the fault segments (Fig. 17). The West Baram fault segments are clearly visible as steeply dipping (9° to 11°) faults with normal offset in the deeper section (*ca* 2000 ms TWT) and several faults penetrate until the seabed (*ca* 200 ms TWT), especially at the neck-point and shelf-edge (Fig. 17B). These younger and prominent WBL fault segments seem to control the Tatau–Suai shelf-edge delta based on proximity between the T-S delta and the faults at the present-day shelf-edge within a 20 km wide zone (Fig. 17B). This study identifies the WBL as a *ca* 20 km wide fault zone with normal offset, which forms part of a regional strike–slip fault system (Morley, 2002).

Upper slope morphologies and geometry

Aside from the fault controls, the sediment bypass to the deep-water is also enhanced by the headward incision process as indicated by a feeder canyon, which causes an irregular shelf-edge and separates the shelf and slope area (Fig. 16D). The enlarged image of the northward area (Fig. 18) shows the upper slope area as high-gradient (>0.1°), deep water (−200 to −900 msl depth), and with a rugged/irregular seabed, compared to the shelf area, which is low-gradient (<0.01°), shallow water (−110 to −130 msl depth), and with a smooth seabed. The feeder canyons are north-east-trending with

© 2023 The Authors. *Sedimentology* published by John Wiley & Sons Ltd on behalf of International Association of Sedimentologists, *Sedimentology*, **71**, 319–354

13653091, 2024, 1, Downloaded from https://onlinelibrary.wiley.com/doi/10.1111/sed.13138 by Test, Wiley Online Library on [22/01/2024]. See the Terms and Conditions (https://onlinelibrary.wiley.com/terms-and-conditions) on Wiley Online Library for rules of use; OA articles are governed by the applicable Creative Commons License

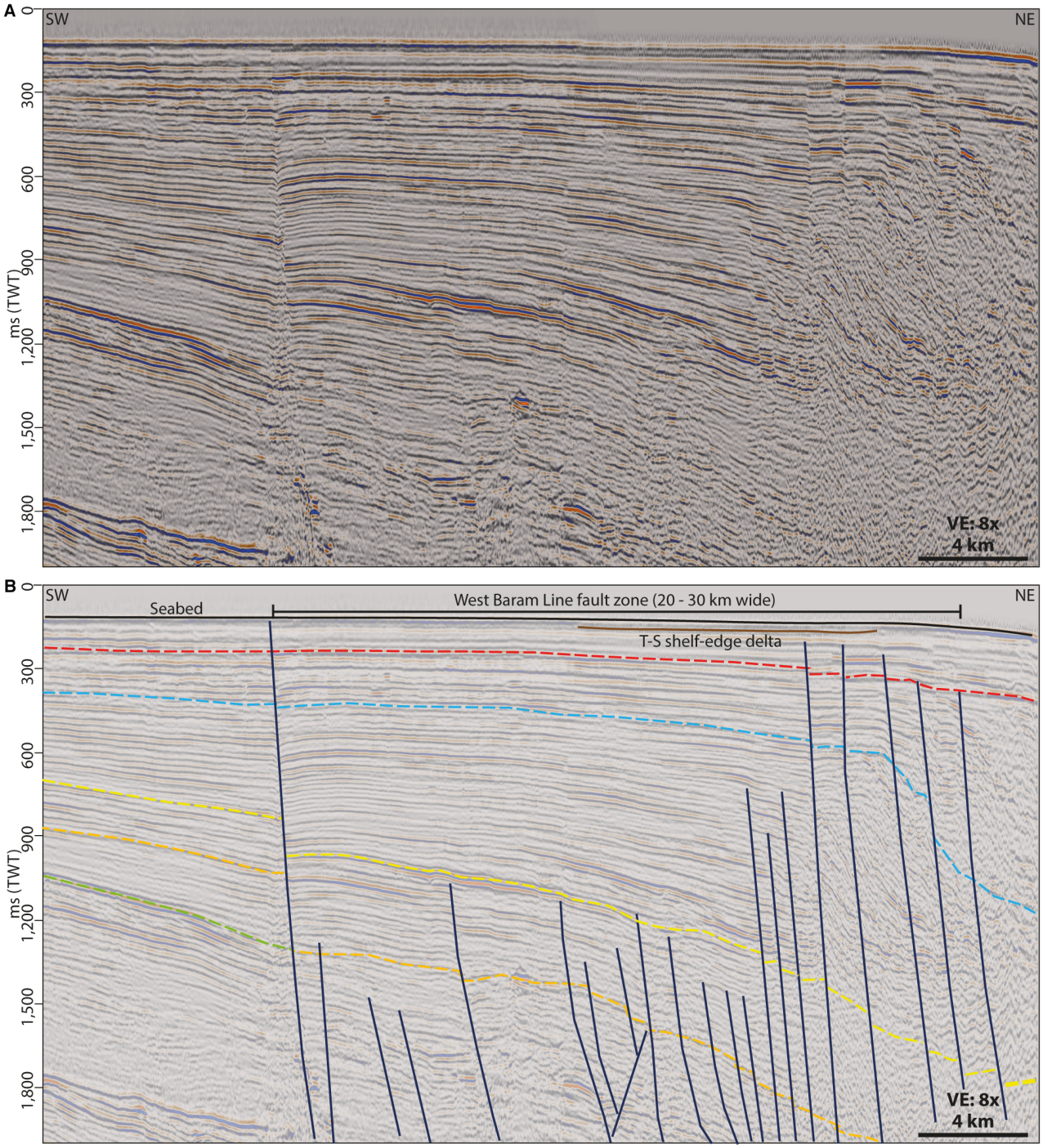


Fig. 17. The seismic section of across the 20 to 30 km wide West Baram Line (WBL) fault zone. Refer to Fig. 16 for location. (A) Uninterpreted. (B) Interpreted seismic section in relation to the shallow Tatau–Suai (T-S) shelf edge delta within *ca* 150 ms TWT. The north-west/south-east lineaments are identified as steeply dipping normal offsets that penetrate very close to the seabed and the T-S shelf edge delta especially towards the south-west and north-east section.

broad (*ca* 1000 to 1700 m wide) headward incision within −140 to −200 msl depth (Fig. 18B). The feeder canyons are also persistently observed in the deeper time-slice map at 70 ms TWT (*ca* 56 m depth) to the shallow time-slice map at 30 ms TWT (*ca* 24 m depth; Fig. 18).

The feeder canyons also transported sediments to the upper slope channels, which are

© 2023 The Authors. *Sedimentology* published by John Wiley & Sons Ltd on behalf of International Association of Sedimentologists, *Sedimentology*, **71**, 319–354

13653091, 2024, 1, Downloaded from https://onlinelibrary.wiley.com/doi/10.1111/sed.13138 by Test, Wiley Online Library on [22/01/2024]. See the Terms and Conditions (https://onlinelibrary.wiley.com/terms-and-conditions) on Wiley Online Library for rules of use; OA articles are governed by the applicable Creative Commons License

specifically referred to as gullies (Fig. 18B). These gullies are observed as a prominent erosional and dense network of dendritic features in the upper slope and described as north-east/north-west trending, very narrow (*ca* 100 to 200 m wide) channels (Fig. 18B). In strike-oriented seismic sections, the feeder canyons are identified as deep incisions within *ca* 180 to 280 ms TWT (*ca* 80 m deep; Fig. 19A). The gullies are identified as shallower incisions within *ca* 600 to 640 ms TWT (*ca* 30 m deep) and characterized by very rugged topography on the present-day seabed (Fig. 19B). These gullies and feeder canyons also possibly cause an unstable shelf-edge by eroding the shelf, in addition to the WBL (Fig. 18B). In summary, the T-S shelf-edge delta is terminated by the northward-dipping WBL fault segments. Sediments reaching the shelf were likely transported to the deep-water through the feeder canyons based on the presence of numerous erosional and dendritic gullies on the steep upper slope (Fig. 18).

DEPOSITIONAL SYNTHESIS AND DISCUSSION

The incised valleys in this study show a typical incised valley dimension for a coastal plain setting (Gibling, 2007; Wang *et al.*, 2019) and similar depositional facies (fluvial, estuarine and shallow marine) with other Quaternary incised valleys in the Sunda Shelf (Darmadi *et al.*, 2007; Reijenstein *et al.*, 2011; Alqahtani *et al.*, 2015; Wetzel *et al.*, 2021), but with different incised valley architecture. This study discovers a two-tier incised valley architecture (Fig. 20), which has never been observed previously in the other Quaternary incised valleys in the Sunda shelf. The incised valley in the Sunda Shelf is typically observed as a single-storey and simple incised valley architecture (Alqahtani *et al.*, 2015). However, a two-tier incised valley architecture can be observed in other analogues such as the Mississippi valley, which comprises compound valley architecture due to multiple fluvial cycles (Blum & Törnqvist, 2000).

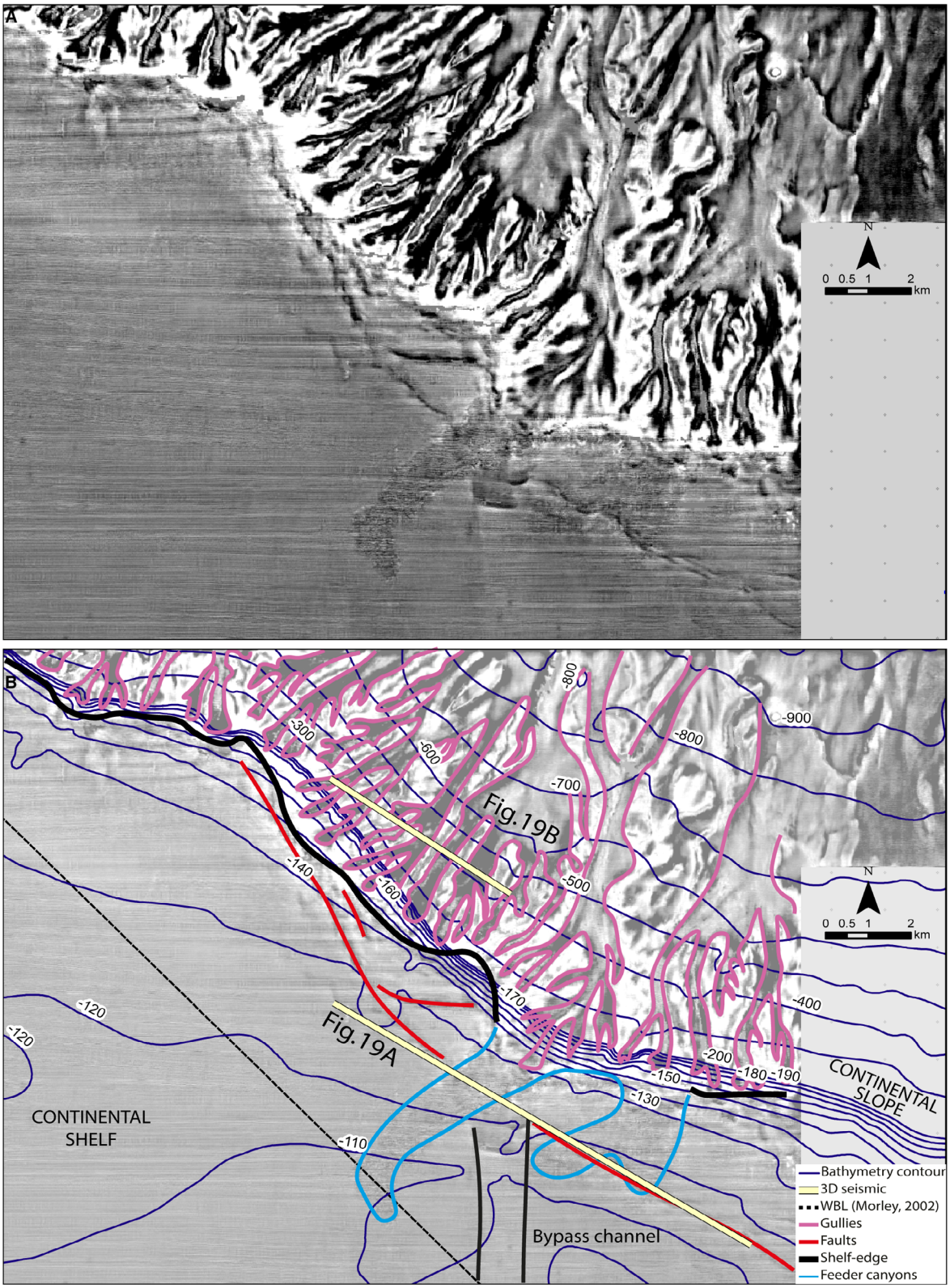
In this study, the two-tier valley architecture is observed in the downstream part of the main incised valley only and is not observed in the tributary Suai incised valley. The Tatau incised valley comprises two-tier valley architecture with two types of fluvial deposits (lower and upper Unit 3.6), whereas the Suai valley comprises a single-tier valley. These similar two types of fluvial deposits are observed in the palaeo-Chao Phraya incised valley as Unit 7, which comprises a basal coarse-grained interval associated with low-sinuosity channels (Unit 7.1) and overlain with two heterolithic shell-bearing intervals (Units 7.2 and 7.3) associated with high-sinuosity channels (Alqahtani *et al.*, 2015). The lower Unit 3.6 is interpreted as a braided river deposit based on amalgamated channel complexes and the upper Unit 3.6 is interpreted as meandering channels based on lateral accretion and valley widening (Fig. 20A; Friend *et al.*, 1979; Miall, 1985; Shanley & McCabe, 1994; Pranter *et al.*, 2009; Alqahtani *et al.*, 2015).

Therefore, the lower Unit 3.6 (lower-tier Tatau incised valley) potentially formed during relative sea-level fall during the initial LGM lowstand phase. In contrast, the upper Unit 3.6 (upper-tier Tatau, Suai incised valley and T-S shelf edge delta) possibly formed during the initial (Late Pleistocene – Early Holocene) transgressive phase (Fig. 20B; Shanley & McCabe, 1994; Hiscott, 2001; Strong & Paola, 2010; Alqahtani *et al.*, 2015; Twarog *et al.*, 2021). The incised valley-fill (Unit 3.6) is overlain by thin (*ca* 3 m thick) transgressive sediments (Unit 4.1), as seen in both high-resolution seismic and boreholes. The relatively thin transgressive sediments in more basinward areas (for example, *ca* 3 m thick in Unit 4.1 in Central Luconia Province) may reflect a combination of reduced sediment supply and/or erosional transgression during Early – Middle Holocene, as seen in other low-gradient shelves (Wetzel *et al.*, 2021).

The authors deduce that two-tier valley architecture is a characteristic for downstream fluvial-dominated incised valley (Willis, 1997; Blum *et al.*, 2013) due to high sediment supply, which can be observed based on valley widening (Martin *et al.*, 2011). The incised valley with high sediment supply also results in shelf-edge delta in the shelf margin (Willis, 1997; Sylvester *et al.*, 2012; Bentley *et al.*, 2016). In this study, the shelf edge delta comprises multiple mouth bars and fluvio-tidal distributary channels within the active and abandoned delta lobes (Wellner *et al.*, 2005). The T-S shelf-edge delta received the sediment from the T-S valley and formed lobate features infilled with mouth bars and fluvio-tidal distributary channels (Fig. 8). The delta plain is commonly dominated by low-sinuosity distributary channels and lobate-shaped sediment bars (Coleman & Wright, 1975; Olariu & Bhattacharya, 2006). The distributary channels

© 2023 The Authors. *Sedimentology* published by John Wiley & Sons Ltd on behalf of International Association of Sedimentologists, *Sedimentology*, **71**, 319–354

13653091, 2024, 1, Downloaded from https://onlinelibrary.wiley.com/doi/10.1111/sed.13138 by Test, Wiley Online Library on [22/01/2024]. See the Terms and Conditions (https://onlinelibrary.wiley.com/terms-and-conditions) on Wiley Online Library for rules of use; OA articles are governed by the applicable Creative Commons License



also responded to the tidal influence as the channels flow close to the palaeo-shoreline (i.e. shelf-edge). The shelf-edge delta is commonly described as tidally influenced facies and prograding clinoform that are cut by distributary channels (Carvajal & Steel, 2009).

© 2023 The Authors. *Sedimentology* published by John Wiley & Sons Ltd on behalf of International Association of Sedimentologists, *Sedimentology*, **71**, 319–354

13653091, 2024, 1, Downloaded from https://onlinelibrary.wiley.com/doi/10.1111/sed.13138 by Test, Wiley Online Library on [22/01/2024]. See the Terms and Conditions (https://onlinelibrary.wiley.com/terms-and-conditions) on Wiley Online Library for rules of use; OA articles are governed by the applicable Creative Commons License

Fig. 18. Flattened time-slice map at 20 ms TWT (*ca* 16 m depth) beneath the seabed of the shelf-edge and upper slope areas. (A) Uninterpreted. (B) Interpreted map shows Tatau–Suai (T-S) shelf-edge delta river mouth/bypass channel on the continental shelf and upper slope channels (feeder canyons, gullies) on the continental slope. The T-S shelf-edge delta feeds the continental slope through the bypass channel and feeder canyons. Sharp north-west/south-east lineaments are identified within the shelf-edge delta area with similar orientation to the irregular shelf-edge delta. Dense gullies form a network in the upper slope with dominant north/north-east orientation, which causes slope erosion cutting the shelf at an irregular shelf-edge within −130 to −200 msl.

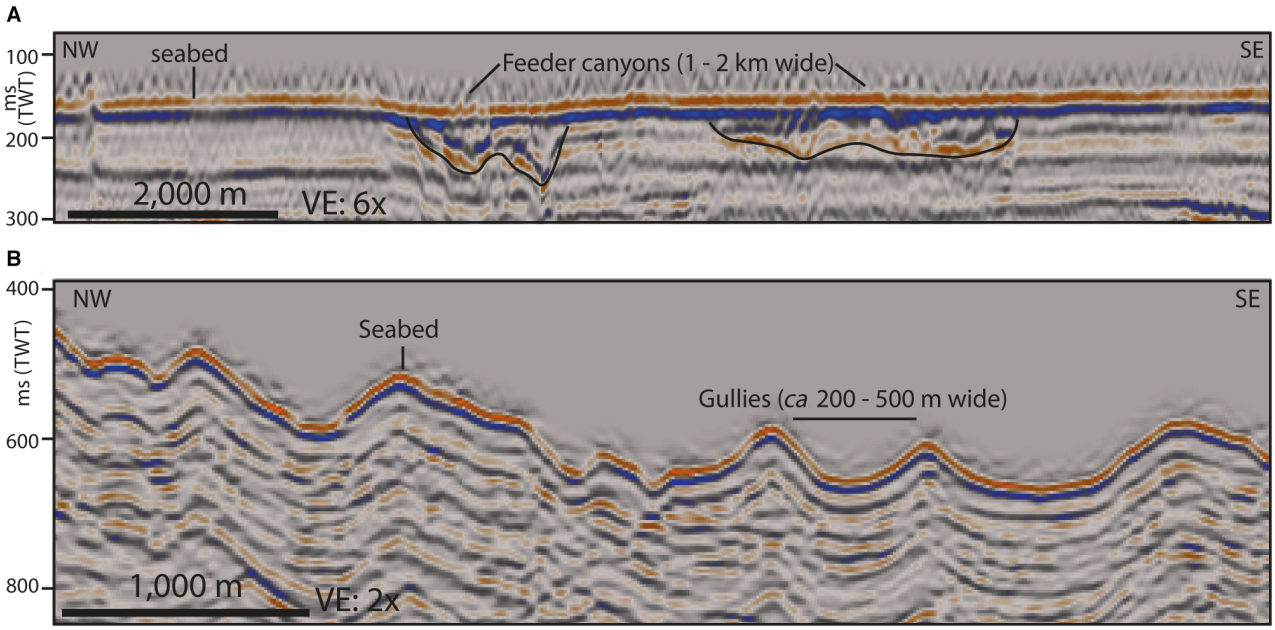


Fig. 19. Seismic sections across the shelf-edge and upper slope channels. (A) Wide and deep (*ca* 1 to 2 km wide, *ca* 80 m deep) feeder canyons at the shelf-edge and smooth seabed; (B) Significant rugose present-day seabed in the upper slope area, which is dominated by narrow and shallower gullies (*ca* 200 to 500 m wide, *ca* 40 m deep). Refer to Fig. 18 for the seismic line locations.

The modern Trusan delta (north-west Borneo), Wax Lake Delta (Mississippi River) and palaeo-Baram shelf-edge delta can be seen as analogues to the T-S shelf-edge delta recognition due to similar fluvio-deltaic morphologies and characteristics. For example, the Trusan Delta shows a transition from a meandering river within a confined valley (freshwater swamp) to low-sinuosity distributary channels in the delta plain (mangrove swamp; Lambiase *et al.*, 2003). The Wax Lake Delta comprises prominent active and abandoned delta lobes, which are made up of small-scale distributary channels and mouth bars (Wellner *et al.*, 2005). The palaeo-Baram shelf-edge delta also can be imagined as an analogue for the T-S shelf-edge delta based on its tectonically-controlled shelf-edge and the presence of slope channels (Hiscott, 2001). The shelf-edge deltas and deep-water morphologies have also been observed along the north-west Borneo margin such as: palaeo-North Sunda river shelf-edge delta and mass transport deposits (Wong *et al.*, 2003; Hanebuth *et al.*, 2011); palaeo-Baram shelf-edge delta (Hiscott, 2001); submarine landslide in the Baram canyon (Gee *et al.*, 2007); and present-day canyons in the continental slope offshore Brunei (Straub *et al.*, 2012). The T-S shelf-edge supplied sediments to the upper slope channels and possibly linked with submarine landslides in the deep-water (Fig. 8).

The lower delta plain area is also cut by several discontinuous north-west/south-east-trending WBL lineaments, which are more numerous in the deeper seismic amplitude map, with increasing frequency towards the shelf edge (Figs 16, 17 and 20). The most palaeo-landward of the north-west/south-east lineaments is also close to the 'neck point' of the valley to lower delta plain

© 2023 The Authors. *Sedimentology* published by John Wiley & Sons Ltd on behalf of International Association of Sedimentologists, *Sedimentology*, **71**, 319–354

13653091, 2024, 1, Downloaded from https://onlinelibrary.wiley.com/doi/10.1111/sed.13138 by Test, Wiley Online Library on [22/01/2024]. See the Terms and Conditions (https://onlinelibrary.wiley.com/terms-and-conditions) on Wiley Online Library for rules of use; OA articles are governed by the applicable Creative Commons License

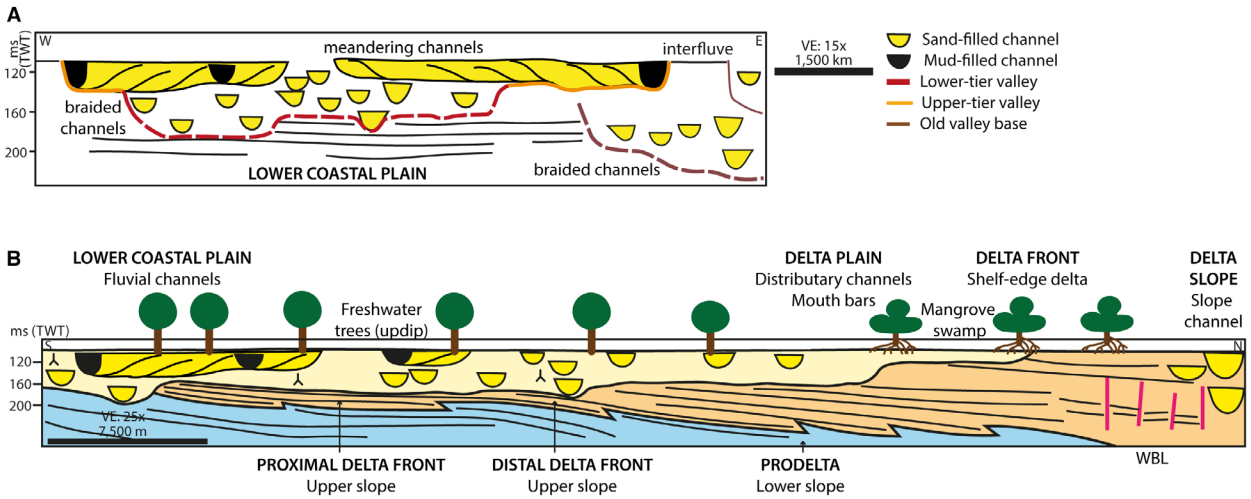


Fig. 20. Schematic interpretation of the Tatau incised valley system. (A) Schematic depositional strike line showing the inferred incised valley fluvial architecture, comprising: (i) confined, narrow and, possibly, isolated sand-filled braided channels in the lower-tier of the valley (base defined by dashed red lines); and (ii) unconfined, wider, meandering channels with point bars and abandoned channel-fills in the upper-tier of the valley (base defined by solid orange line). (B) Schematic depositional dip line in a downstream position showing an incised valley to the left (relatively landward) and its downstream termination and interfingering relationship with shelf-edge delta to upper slope deposits (to the right – relatively basinward). The lower-coastal plain comprises a thick (*ca* 60 m) fluvial unit dominated with freshwater trees/tropical rainforest in the up-dip area (left) and thinning to *ca* 8 to 25 m thick in the down-dip area (right). The delta front thickens basinward, is dominated by mangrove swamps and overlies prodelta–upper slope deposits.

boundary. Features with a prominent north-west/south-east trend may all be related to the WBL (Morley, 2002) and most likely mark a 10 to 20 km wide near-surface zone of deformation, including slump scars at the Late Pleistocene shelf edge. The 'neck point' or transition area, where the confined T-S valleys merge (to the south-west and south-east) and expand into an unconfined shelf-edge delta setting (to the north-east), possibly signifies a zone of deep incision. Channel sinuosity also decreases abruptly to the north-east of the 'neck point' and could mark the onset of tectonic influence of the WBL. The most striking feature of the 'neck point' is the change from high-sinuosity channels in the south (in both Tatau and Suai incised valleys) to less sinuous channel patterns in the north (Fig. 8). The present-day shelf edge might signify some delta front accretion across the WBL (Hiscott, 2003). This combination indicates fault-induced slumping (i.e. WBL related) and shelf edge instability due to high rates of sediment supply, consistent with the WBL/shelf edge being a zone of several kilometres width (*ca* 10 to 20 km; Steel *et al.*, 2003).

This study interpreted that the Tatau–Suai incised valleys and shelf-edge delta in the eastern CLP are mainly influenced by tectonics (i.e. WBL), which is recognized as a *ca* 20 to 30 km wide fault zone. The north-west Borneo hinterland has recently been uplifted during Pliocene and caused subsidence in the CLP and was also influenced by the WBL (Koša, 2015). In this study, the WBL is observed to have steeply-dipping normal fault offsets within the Plio-Pleistocene succession and is still active until today. The north-west/south-east fault segments were observed to penetrate the seabed especially at the shelf-edge and cause headward incision in the upper slope. The WBL is also identified as a *ca* 20 to 30 km wide fault zone from the 'neck point' to the shelf-edge. The effect of shelf subsidence due to the WBL can be observed based on the palaeo-Tatau valley direction, in which the upstream valley initially flows northward and suddenly changes its direction towards the north-east in the midstream to downstream valley. The WBL has also terminated the shelf-edge delta based on numerous north-west/south-east lineaments at the margin of the abandoned delta lobes. This relationship possibly explains the lobe switching from the westward progradation to northward progradation as shown by the active T-S delta lobe.

© 2023 The Authors. *Sedimentology* published by John Wiley & Sons Ltd on behalf of International Association of Sedimentologists, *Sedimentology*, **71**, 319–354

13653091, 2024, 1, Downloaded from https://onlinelibrary.wiley.com/doi/10.1111/sed.13138 by Test, Wiley Online Library on [22/01/2024]. See the Terms and Conditions (https://onlinelibrary.wiley.com/terms-and-conditions) on Wiley Online Library for rules of use; OA articles are governed by the applicable Creative Commons License

Subsidence also creates more accommodation space, increases sediment thickness (Shanley & McCabe, 1994; Yan *et al.*, 2020) and thus explains the presence of *ca* 1 km thick prograding sediment wedges in the Sunda Shelf margin (Hiscott, 2001; Hanebuth *et al.*, 2003). Similarly, the tectonic control on the basin sedimentation is reported in the Bunguran Trough (West Luconia Delta Province), where extensional and strike–slip faulting of the West Balingian Line has caused basin formation and subsidence (Madon & Jong, 2022). Thus, this study shows that the WBL is still active, based on the present-day shelf-edge morphologies, which plays a major role in controlling Plio-Pleistocene sedimentation and present-day upper slope process in the CLP.

CONCLUSIONS

1 The Late Quaternary stratigraphic succession of the Central Luconia – Balingian provinces (Central Luconia – Balingian; off the coast of Sarawak) comprises a network of approximately ten incised valleys that terminate in multiple shelf-edge deltas at the shelf margin, which coincides with the tectonically active West Baram Line (WBL).

2 The main morphological characteristics of the incised valleys are as follows: (i) the dominant trend is south to north; (ii) *ca* 300 to 12 000 m wide, with width increasing downstream to a maximum at the shelf edge, (iii) mostly low sinuosity (SI = 1); and (iv) *ca* 20 to 60 m deep.

3 The stratigraphic architecture of the incised valleys is divided into two stratigraphic levels ('tiers'): (i) the lower tier valley is relatively narrow, infilled with low sinuosity channels and is interpreted to have formed during the last glacial maximum (LGM) lowstand; (ii) the upper tier is relatively wide and filled with high sinuosity channels with brackish water influence and is interpreted to have formed during sea-level rise, possibly marking the initial phase of the Late Pleistocene transgression.

4 Incised valley formation was primarily linked to relative sea-level fall in the Late Pleistocene, during the LGM. Other controls include hinterland uplift during the Pliocene and tectonic movement along the WBL. However, the Central Luconia – Balingian area was largely tectonically stable.

5 Quaternary valleys can be connected upstream with their present-day equivalents in onshore Sarawak to reconstruct palaeo-Tatau drainage area.

ACKNOWLEDGEMENTS

The first author is grateful to the Universiti Terengganu Malaysia for providing a PhD scholarship. The authors are grateful to PETRONAS (MPM & Geomatics departments) for providing the 3D seismic data, Halliburton Landmark and Eliis Paleoscan for the university software grants. Finally, we would like to thank Christopher Fielding, Alessandro Amorosi and an anonymous reviewer for their constructive feedback.

CONFLICT OF INTEREST

The authors declare that they have no known competing interests that could have appeared to influence the work reported in this paper.

DATA AVAILABILITY STATEMENT

The data that support the findings of this study are available from the corresponding author upon reasonable request.

REFERENCES

Ali, M.Y. and **Abolins, P.** (1999) Central Luconia Province. In: *The Petroleum Geology and Resources of Malaysia*, pp. 369–392. PETRONAS, Kuala Lumpur.

Alqahtani, F.A., **Johnson, H.D.**, **Jackson, C.A.L.** and **Som, M.R.B.** (2015) Nature, origin and evolution of a Late Pleistocene incised valley-fill, Sunda Shelf, Southeast Asia. *Sedimentology*, **62**, 1198–1232.

Alqahtani, F.A., **Jackson, C.A.-L.**, **Johnson, H.D.** and **Som, M.R.B.** (2017) Controls on the geometry and evolution of humid-tropical fluvial systems: insights from 3D seismic geomorphological analysis of the malay basin, Sunda Shelf, Southeast Asia. *J. Sediment. Res.*, **87**, 17–40.

Bentley, S.J., **Blum, M.D.**, **Maloney, J.**, **Pond, L.** and **Paulsell, R.** (2016) The Mississippi River source-to-sink system: perspectives on tectonic, climatic, and anthropogenic influences, Miocene to Anthropocene. *Earth-Sci. Rev.*, **153**, 139–174.

Best, J.L. and **Ashworth, P.J.** (1997) Scour in large braided rivers and the recognition of sequence stratigraphic boundaries. *Nature*, **387**, 275–277.

Bhattacharya, J.P., **Copeland, P.**, **Lawton, T.F.** and **Holbrook, J.** (2016) Estimation of source area, river paleo-discharge, paleoslope, and sediment budgets of linked deep-time depositional systems and implications for hydrocarbon potential. *Earth-Sci. Rev.*, **153**, 77–110.

Bian, Y.P., **Jian, Z.M.**, **Weng, C.Y.**, **Kuhnt, W.**, **Bolliet, T.** and **Holbourn, A.** (2011) A palynological and palaeoclimatological record from the southern Philippines since the Last Glacial Maximum. *Chin. Sci. Bull.*, **56**, 2359–2365.

© 2023 The Authors. *Sedimentology* published by John Wiley & Sons Ltd on behalf of International Association of Sedimentologists, *Sedimentology*, **71**, 319–354

13653091, 2024, 1, Downloaded from https://onlinelibrary.wiley.com/doi/10.1111/sed.13138 by Test, Wiley Online Library on [22/01/2024]. See the Terms and Conditions (https://onlinelibrary.wiley.com/terms-and-conditions) on Wiley Online Library for rules of use; OA articles are governed by the applicable Creative Commons License

Blum, M.D. and **Törnqvist, T.E.** (2000) Fluvial responses to climate and sea-level change: a review and look forward. *Sedimentology*, **47**, 2–48.

Blum, M., **Martin, J.**, **Milliken, K.** and **Garvin, M.** (2013) Paleovalley systems: insights from quaternary analogs and experiments. *Earth-Sci. Rev.*, **116**, 128–169.

Carvajal, C. and **Steel, R.** (2009) Shelf-Edge architecture and bypass of sand to deep water: influence of shelf-edge processes, sea level, and sediment supply. *J. Sediment. Res.*, **79**, 652–672.

Catuneanu, O., **Abreu, V.**, **Bhattacharya, J.P.**, **Blum, M.D.**, **Dalrymple, R.W.**, **Eriksson, P.G.**, **Fielding, C.R.**, **Fisher, W.L.**, **Galloway, W.E.**, **Gibling, M.R.**, **Giles, K.A.**, **Holbrook, J.M.**, **Jordan, R.**, **Kendall, C.G.S.C.**, **Macurda, B.**, **Martinsen, O.J.**, **Miall, A.D.**, **Neal, J.E.**, **Nummedal, D.**, **Pomar, L.**, **Posamentier, H.W.**, **Pratt, B.R.**, **Sarg, J.F.**, **Shanley, K.W.**, **Steel, R.J.**, **Strasser, A.**, **Tucker, M.E.** and **Winker, C.** (2009) Towards the standardization of sequence stratigraphy. *Earth-Sci. Rev.*, **92**, 1–33.

Coleman, J.M. and **Wright, L.D.** (1975) Modern river deltas: variability of processes and sand bodies.

Cullen, A.B. (2010) Transverse segmentation of the Baram-Balabac Basin, NW Borneo: refining the model of Borneo's tectonic evolution. *Petrol. Geosci.*, **16**, 3–29.

Dalrymple, R.W. (1994) Incised-valley systems: origin and sedimentary sequences. *SEPM Special Publication*, **391**.

Darmadi, Y., **Willis, B.J.** and **Dorobek, S.L.** (2007) Three-dimensional seismic architecture of fluvial sequences on the low-gradient sunda shelf, Offshore Indonesia. *J. Sediment. Res.*, **77**, 225–238.

Epting, M. (1980) Sedimentology of Miocene Carbonate Buildups of Offshore Sarawak.pdf. 17–30.

Friend, F., **Slater, M.J.** and **Williams, R.C.** (1979) Vertical and lateral building. *J. Geol. Soc. London*, **136**, 39–46.

Gee, M.J.R., **Uy, H.S.**, **Warren, J.**, **Morley, C.K.** and **Lambiase, J.J.** (2007) The Brunei slide: a giant submarine landslide on the North West Borneo Margin revealed by 3D seismic data. *Mar. Geol.*, **246**, 9–23.

Gibling, M.R. (2007) Width and thickness of fluvial channel bodies and valley fills in the geological record: a literature compilation and classification. *J. Sediment. Res.*, **76**, 731–770.

Hageman, H. (1987) Paleobathymetrical changes in NW Sarawak during the Oligocene to Pliocene. *Geol. Soc. Malaysia Bull.*, **21**, 91–102.

Hampson, G.J., **Da Vies, S.J.**, **Elliott, T.**, **Flint, S.S.** and **Stollhofen, H.** (1999) Incised valley fill sandstone bodies in Upper Carboniferous fluvio-deltaic strata: recognition and reservoir characterization of Southern North Sea analogues. *Petrol. Geol. Conf. Proc.*, **5**, 771–788.

Hanebuth, T.J.J. and **Stattegger, K.** (2004) Depositional sequences on a late Pleistocene-Holocene tropical siliciclastic shelf (Sunda Shelf, southeast Asia). *J. Asian Earth Sci.*, **23**, 113–126.

Hanebuth, T.J., **Stattegger, K.** and **Saito, Y.** (2002) The stratigraphic architecture of the central Sunda Shelf (SE Asia) recorded by shallow-seismic surveying. *Geo-Mar. Lett.*, **22**, 86–94.

Hanebuth, T.J.J., **Stattegger, K.**, **Schimanski, A.**, **Lüdmann, T.** and **Wong, H.K.** (2003) Late Pleistocene forced-regressive deposits on the Sunda Shelf (Southeast Asia). *Mar. Geol.*, **199**, 139–157.

Hanebuth, T.J.J., **Voris, H.K.**, **Yokoyama, Y.**, **Saito, Y.** and **Okuno, J.** (2011) Formation and fate of sedimentary depocentres on Southeast Asia's Sunda Shelf over the past sea-level cycle and biogeographic implications. *Earth-Sci. Rev.*, **104**, 92–110.

Hiscott, R. (2001) Depositional sequences controlled by high rates of sediment supply, sea-level variations, and growth faulting: the Quaternary Baram Delta of northwestern Borneo.

Hiscott, R. (2003) Latest quaternary Baram Prodelta, Northwestern Borneo. In: *Tropical Deltas of Southeast Asia—Sedimentology, Stratigraphy, and Petroleum Geology* (Eds Sidi, F.H., Nummedal, D., Imbert, P., Darman, H. and Posamentier, H.W.), **76**, pp. 89–107. SEPM (Society for Sedimentary Geology), OK, USA.

Ho, K.F. (1978) Stratigraphic framework for oil exploration in Sarawak. *Geol. Soc. Malaysia Bull.*, **10**, 1–13.

Hutchison, C.S. (2004) Marginal basin evolution: The southern South China Sea. *Mar. Petrol. Geol.*, **21**, 1129–1148.

Hutchison, C.S. (2005) Geology of North-West Borneo.

Iyer, S. (2019) Sarawak Basin: Tectono-Stratigraphic Provinces and their seismic expressions. In: *Geophysical Applications in Malaysia Basins*, pp. 105–134. PETRONAS, Kuala Lumpur.

Koša, E. (2015) Sea-level changes, shoreline journeys, and the seismic stratigraphy of Central Luconia, Miocene-present, offshore Sarawak, NW Borneo. *Mar. Petrol. Geol.*, **59**, 35–55.

Lambiase, J.J. and **Cullen, A.B.** (2013) Sediment supply systems of the Champion "Delta" of NW Borneo: implications for deepwater reservoir sandstones. *J. Asian Earth Sci.*, **76**, 356–371.

Lambiase, J.J., **Damit, A.R.**, **Simmons, M.D.**, **Abdoerrias, R.** and **Hussin, A.** (2003) A depositional model and the stratigraphic development of modern and ancient tide-dominated deltas in NW Borneo. In: *Tropical Deltas of Southeast Asia—Sedimentology, Stratigraphy, and Petroleum Geology* (Eds Sidi, F.H., Nummedal, D., Imbert, P., Darman, H. and Posamentier, H.W.), **76**, pp. 109–123. SEPM (Society for Sedimentary Geology), OK, USA.

Levell, B.K. (1987) The nature and significance of regional unconformities in the hydrocarbon-bearing Neogene sequence offshore West Sabah. *Bull. Geol. Soc. Malaysia*, **21**, 55–90.

Li, L., **Li, Q.**, **Tian, J.**, **Wang, H.** and **Wang, P.** (2013) Low latitude hydro-climatic changes during the Plio-Pleistocene: evidence from high resolution alkane records in the southern South China Sea. *Quatern. Sci. Rev.*, **78**, 209–224.

Lonergan, L., **Maidment, S.C.R.** and **Collier, J.S.** (2006) Pleistocene subglacial tunnel valleys in the central North Sea basin: 3-D morphology and evolution. *J. Quatern. Sci.*, **21**, 891–903.

Lunne, T. (2012) The Fourth James K. Mitchell Lecture: the CPT in offshore soil investigations—a historic perspective. *Geomech. Geoeng.*, **7**, 75–101.

Lunt, P. and **Madon, M.** (2017) A review of the Sarawak Cycles: history and modern application.

Madon, M. (1999) Geological setting of Sarawak. In: *The Petroleum Geology and Resources of Malaysia*, pp. 275–290. PETRONAS, Kuala Lumpur.

Madon, M. and **Abolins, P.** (1999) Balingian province. In: *The Petroleum Geology and Resources of Malaysia*, pp. 343–368. PETRONAS, Kuala Lumpur.

Madon, M. and **Jong, J.** (2022) The crustal structure and evolution of the Bunguran Trough, offshore Sarawak, Malaysia. *Marine and Petroleum Geology*, **139**, 105608.

Madon, M., **Kim, C.L.** and **Wong, R.** (2013) The Structure and Stratigraphy of Deepwater Sarawak, Malaysia: implications for tectonic evolution. *Journal of Asian*

13653091, 2024, 1, Downloaded from https://onlinelibrary.wiley.com/doi/10.1111/sed.13138 by Test, Wiley Online Library on [22/01/2024]. See the Terms and Conditions (https://onlinelibrary.wiley.com/terms-and-conditions) on Wiley Online Library for rules of use; OA articles are governed by the applicable Creative Commons License

Earth Sciences, **76**, 312–333. ttps://doi.org/10.1016/j.jseaes.2013.04.040.

Martin, J., **Cantelli, A.**, **Paola, C.**, **Blum, M.** and **Wolinsky, M.** (2011) Quantitative modeling of the evolution and geometry of incised valleys. *J. Sediment. Res.*, **81**, 64–79.

Mattheus, C.R. and **Rodriguez, A.B.** (2011) Controls on late quaternary incised-valley dimension along passive margins evaluated using empirical data. *Sedimentology*, **58**, 1113–1137.

Miall, A.D. (1985) Architectural-element analysis: a new method of facies analysis applied to fluvial deposits. *Earth Sci. Rev.*, **22**, 261–308.

Miall, A.D. (2002) Fluvial systems in the Malay time-slice analysis. *Am. Assoc. Petrol. Geol. Bull.*, **7**, 1201–1216.

Milliman, J.D. and **Syvitski, J.P.M.** (1992) Geomorphic/tectonic control of sediment discharge to the ocean: the importance of small mountainous rivers. *J. Geol.*, **100**, 525–544.

Morley, C.K. (2002) A tectonic model for the Tertiary evolution of strike-slip faults and rift basins in SE Asia. *Tectonophysics*, **347**, 189–215.

Morley, R.J. (2013) Cenozoic ecological history of South East Asian peat mires based on the comparison of coals with present day and late quaternary peats. *J. Limnol.*, **72**, 36–59.

Morley, C.K. (2016) Major unconformities/termination of extension events and associated surfaces in the South China Seas: review and implications for tectonic development. *J. Asian Earth Sci.*, **120**, 62–86.

Olariu, C. and **Bhattacharya, J.P.** (2006) Terminal distributary channels and delta front architecture of river-dominated delta systems. *J. Sediment. Res.*, **76**, 212–233.

PETRONAS. (2013) Geotechnical Investigation Report. Unpublished report.

PETRONAS. (2019) Geophysical Applications in Malaysian Basins. Unpublished report.

Posamentier, H.W. (2001) Lowstand alluvial bypass systems: Incised vs. unincised. *AAPG Bulletin*, **10**, 1771–1793.

Posamentier, H.W., **Jervey, M.T.** and **Vail, P.R.** (1988) Eustatic controls on clastic deposition I—conceptual framework. In: *Sea-Level Changes: An Integrated Approach* (Eds Wilgus, C.K., Hastings, B.S., Posamentier, H., Wagoner, J.V., Ross, C.A. and Kendall, C.G.S.C.), **42**, pp. 125–154. SEPM (Society for Sedimentary Geology), OK, USA.

Pranter, M.J., **Cole, R.D.**, **Panjaitan, H.** and **Sommer, N.K.** (2009) Sandstone-body dimensions in a lower coastal-plain depositional setting: Lower Williams Fork formation, Coal Canyon, Piceance Basin, Colorado. *Am. Assoc. Petrol. Geol. Bull.*, **93**, 1379–1401.

Prins, L.T. and **Andresen, K.J.** (2021) A geotechnical stratigraphy for the shallow subsurface in the Southern Central Graben, North Sea. *Eng. Geol.*, **286**, 106089.

Puchała, R.J., **Porbski, S.J.**, **Śliwiński, W.R.** and **August, C.J.** (2011) Pleistocene to Holocene transition in the central basin of the Gulf of Thailand, based on geoacoustic survey and radiocarbon ages. *Mar. Geol.*, **288**, 103–111.

Reijenstein, H.M., **Posamentier, H.W.** and **Bhattacharya, J.P.** (2011) Seismic geomorphobgy and high-resolution seismic stratigraphy of inner-shelf fluvial, estuarine, deltaic, and marine sequences, Gulf of Thailand. *AAPG Bull.*, **95**, 1959–1990.

Reynaud, J.-Y., **Tessier, B.**, **Proust, J.-N.**, **Dalrymple, R.W.**, **Bourillet, J.-F.**, **De Batist, M.**, **Lericolais, G.**, **Berne, S.** and **Marsset, T.** (1999) Architecture and sequence stratigraphy of a late Neogene incised valley at the shelf margin, southern Celtic Sea. *J. Sediment. Res.*, **69**, 351–364.

Samorn, H. (2006) Fluvial Reservoir Architecture from near-Surface 3D Seismic Data, Block B8/32, Gulf of Thailand.

Sathiamurthy, E. and **Voris, K.H.** (2006) Maps of Holocene Sea Level Transgression and Submerged Lakes on the Sunda Shelf. 1–44 pp.

Schiltz, M. (2020) On the use of cpts in stratigraphy: Recent observations and some illustrative cases. *Geol. Belgica*, **23**, 1–13.

Shanley, K.W. and **McCabe, P.J.** (1994) Perspectives on the sequence stratigraphy of continental strata. *Am. Assoc. Petrol. Geol. Bull.*, **78**, 544–568.

Staub, J.R. and **Gastaldo, R.A.** (2003) Late quaternary sedimentation and peat development in the Rajang River Delta, Sarawak, East Malaysia. In: *Tropical Deltas of Southeast Asia—Sedimentology, Stratigraphy, and Petroleum Geology* (Eds Sidi, F.H., Nummedal, D., Imbert, P., Darman, H. and Posamentier, H.W.), **76**, pp. 71–87. SEPM (Society for Sedimentary Geology), OK, USA.

Steel, R., **Plink-Björklund, P.**, **Porębski, S.J.**, **Mellere, D.** and **Maija, S.** (2003) *Shelf-Edge Delta Types and their Sequence-Stratigraphic Relationships*, pp. 205–230. GCSSEPM Special Publication.

Stewart, M.A., **Lonergan, L.** and **Hampson, G.** (2013) 3D seismic analysis of buried tunnel valleys in the central North Sea: Morphology, cross-cutting generations and glacial history. *Quatern. Sci. Rev.*, **72**, 1–17.

Straub, K.M., **Mohrig, D.** and **Pirmez, C.** (2012) Architecture of an Aggradational tributary submarine-channel network on the continental slope Offshore Brunei Darussalam. In: *Application of the Principles of Seismic Geomorphology to Continental-Slope and Base-of-Slope Systems: Case Studies from Seafloor and Near-Seafloor Analogues*, **99**, pp. 13–30. SEPM (Society for Sedimentary Geology), OK, USA.

Strong, N. and **Paola, C.** (2010) Valleys that never were: time surfaces versus stratigraphic surfaces-reply. *J. Sediment. Res.*, **80**, 4–5.

Sylvester, Z., **Pirmez, C.** and **Cantelli, A.** (2012) Seismic stratigraphy of a shelf-edge delta and linked submarine channels in the Northeastern Gulf of Mexico. *Mar. Petrol. Geol.*, **28**, 716–727.

Tan, D.N.K., **Rahman, A.H.A.**, **Anuar, A.**, **Bait, B.** and **Tho, C.K.** (1999) West Baram Delta. In: *The Petroleum Geology and Resources of Malaysia*, pp. 291–343. PETRONAS, Kuala Lumpur.

Tanabe, S., **Saito, Y.**, **Lan, V.**, **Q.**, **Hanebuth, T.J.J.**, **Lan Ngo, Q.** and **Kitamura, A.** (2006) Holocene evolution of the Song Hong (Red River) delta system, northern Vietnam. *Sed. Geol.*, **187**, 29–61.

Thanh, N.T., **Cuong, D.H.**, **Stattegger, K.**, **Dung, B.V.**, **Yang, S.**, **Chi, N.T.K.**, **Tung, N.X.**, **Tinh, N.V.** and **Nga, N.T.** (2021) Depositional sequences of the Mekong river delta and adjacent shelf over the past 140 kyr, southern Vietnam. *J. Asian Earth Sci.*, **206**, 104634.

Ting, K.K., **Tan, Y.E.**, **Chiew, E.**, **Lee, E.L.**, **Azudin, A.N.** and **Ishak, N.A.** (2021) Assessing controls on isolated carbonate platform development in Central Luconia, NW Borneo, from a regional 3D seismic facies and geomorphology investigation.

Tjallingii, R., **Stattegger, K.**, **Wetzel, A.** and **Phach, P.** (2010) Infilling and flooding of the Mekong River incised valley during deglacial sea-level rise. *Quatern. Sci. Rev.*, **29**, 1432–1444.

Truong, M.H., **Nguyen, V.L.**, **Ta, T.K.O.** and **Takemura, J.** (2011) Changes in late Pleistocene-Holocene sedimentary

© 2023 The Authors. *Sedimentology* published by John Wiley & Sons Ltd on behalf of International Association of Sedimentologists, *Sedimentology*, **71**, 319–354

13653091, 2024, 1, Downloaded from https://onlinelibrary.wiley.com/doi/10.1111/sed.13138 by Test, Wiley Online Library on [22/01/2024]. See the Terms and Conditions (https://onlinelibrary.wiley.com/terms-and-conditions) on Wiley Online Library for rules of use; OA articles are governed by the applicable Creative Commons License

facies of the Mekong River Delta and the influence of sedimentary environment on geotechnical engineering properties. *Eng. Geol.*, **122**, 146–159.

Twarog, M.R., **Culver, S.J.**, **Mallinson, D.J.**, **Leorri, E.**, **Donovan, B.**, **Harrison, E.I.**, **Hindes, H.**, **Reed, D.**, **Horsman, E.**, **Shazili, N.A.M.** and **Parham, P.R.** (2021) Depositional environments and sequence stratigraphy of post-last glacial maximum incised valley-fill, Malay Basin, northern Sunda Shelf. *Mar. Geol.*, **436**, 106457.

Van Vliet, A. and **Wannier, M.** (2023) Exploration history of the Central Luconia Carbonate Gas Play. In: *Cenozoic Isolated Carbonate Platforms—Focus Southeast Asia* (Eds Rankey, E.C. and Pöppelreiter, M.C.), **114**, pp. 192–206. SEPM Special Publication.

Van Wagoner, J.C., **Mitchum, R.M.**, **Campion, K.M.** and **Rahmanian, V.D.** (1990) Siliciclastic sequence stratigraphy in well logs, cores, and outcrops: Concepts for high-resolution correlation of time and facies. *AAPG Spec. Vol.*, **174**, 55.

Voris, H.K. (2000) Maps of Pleistocene sea levels in Southeast Asia: Shorelines, river systems and time durations. *J. Biogeogr.*, **27**, 1153–1167.

Wang, R., **Colombera, L.** and **Mountney, N.P.** (2019) Geological controls on the geometry of incised-valley fills: insights from a global dataset of late-Quaternary examples. *Sedimentology*, **66**, 2134–2168.

Wellner, R., **Beaubouef, R.**, **Van Wagoner, J.**, **Roberts, H.** and **Sun, T.** (2005) Jet-Plume depositional bodies - The primary building blocks of Wax Lake Delta. *Gulf Coast Assoc. Geol. Soc. Trans*, **55**, 867–909.

Wetzel, A. (2017) Sedimentological and ichnological implications of rapid Holocene flooding of a gently sloping mud-dominated incised valley - an example from the Red River (Gulf of Tonkin). *Sedimentology*, **64**, 1173–1202.

Wetzel, A., **Feldens, A.**, **Unverricht, D.**, **Stattegger, K.** and **Tjallingii, R.** (2021) Late Pleistocene sea-level changes and the formation and fill of bent valleys incised into the shelf of the western South China Sea. *J. Asian Earth Sci.*, **206**, 104626.

Willis, B.J. (1997) Architecture of fluvial-dominated valley-fill deposits in the Cretaceous Fall River Formation. *Sedimentology*, **44**, 735–757.

Wong, H.K., **Lüdmann, T.**, **Haft, C.**, **Paulsen, A.-M.**, **Hübscher, C.** and **Geng, J.** (2003) Quaternary sedimentation in the Molengraaff Paleo-Delta, Northern Sunda Shelf (Southern South China Sea). In: *Tropical Deltas of Southeast Asia—Sedimentology, Stratigraphy, and Petroleum Geology* (Eds Sidi, F.H., Nummedal, D., Imbert, P., Darman, H. and Posamentier, H.W.), **76**, pp. 201–216. SEPM (Society for Sedimentary Geology), OK, USA.

Wurster, C.M., **Rifai, H.**, **Zhou, B.**, **Haig, J.** and **Bird, M.I.** (2019) Savanna in equatorial Borneo during the late Pleistocene. *Sci. Rep.*, **9**, 1–7.

Yan, N., **Colombera, L.** and **Mountney, N.P.** (2020) Three-dimensional forward stratigraphic modelling of the sedimentary architecture of meandering-river successions in evolving half-graben rift basins. *Basin Res.*, **32**, 68–90.

Zaitlin, B.A., **Dalrymple, R.W.** and **Boyd, R.** (1994) The stratigraphic organization of incised-valley systems associated with relative sea-level change. In: *Incised-Valley Systems: Origin and Sedimentary Sequences* (Eds Dalrymple, R.W., Boyd, R. and Zaitlin, B.A.), **51**, pp. 45–59. SEPM (Society for Sedimentary Geology), OK, USA.

Zeng, H. (2007) Seismic imaging for seismic geomorphology beyond the seabed: potentials and challenges. *Geol. Soc. Lond. Spec. Publ.*, **277**, 15–28.

Manuscript received 17 April 2023; revision accepted 8 September 2023

© 2023 The Authors. *Sedimentology* published by John Wiley & Sons Ltd on behalf of International Association of Sedimentologists, *Sedimentology*, **71**, 319–354

13653091, 2024, 1, Downloaded from https://onlinelibrary.wiley.com/doi/10.1111/sed.13138 by Test, Wiley Online Library on [22/01/2024]. See the Terms and Conditions (https://onlinelibrary.wiley.com/terms-and-conditions) on Wiley Online Library for rules of use; OA articles are governed by the applicable Creative Commons License